Stony Brook University

Osteopenia Uncovered by Remodeling in Spatial Distribution of Elastic Moduli in Orthogonal Orientations-A Nanoindentation Study

A Thesis Presented

by

Kartikey Grover

to

The Graduate School

in Partial Fulfillment of the

Requirements

for the Degree of

Master of Science

in

Biomedical Engineering

Stony Brook University

May 2015

Stony Brook University

The Graduate School

Kartikey Grover

We, the thesis committee for the above candidate for the

Master of Science degree, hereby recommend

acceptance of this thesis.

Dr. Yi-Xian Qin (Advisor)
Professor, Department of Biomedical Engineering

Dr. Wei Lin
Associate Professor, Department of Biomedical Engineering

Dr. Balaji Sitharman
Associate Professor, Department of Biomedical Engineering

This thesis is accepted by the Graduate School

Charles Taber
Dean of the Graduate School

Abstract of the Thesis

Osteopenia Uncovered by Remodeling in Spatial Distribution of Elastic Moduli in Orthogonal Orientations-A Nanoindentation Study

by

Kartikey Grover

Master of Science

in

Biomedical Engineering

Stony Brook University

2015

Bone disuse leads to severe bone loss and deterioration of bone architecture. In our study we initially assessed the local distribution of mechanical properties of bone on a micro-nano scale and its correlation to strain distribution. Then the effects of disuse were investigated by investigating remodeling of mechanical properties of bone in the three orthogonal directions. Left tibia samples were obtained from 5-month old female Sprague Dawley rats, including baseline control (n=9) and hindlimb suspended (n=9) groups. Elastic modulus was measured by nanoindentation at the dedicated locations. Three additional tibias from control rats were loaded axially to measure bone strain, with 6-10N at 1Hz on a Bose machine for strain measurements. In the control group, the difference of the elastic modulus between periosteum and endosteum was much higher at the anterior and posterior regions (2.6GPa), where higher strain differences were observed (45με). Minimum elastic modulus difference between periosteum and endosteum was observed at the medial region (0.2GPa), where neutral axis of the strain distribution was oriented with lower strain difference (5με). Strong correlation between elastic modulus difference and strain difference in anterior, posterior, and medial regions was observed (R^2>0.95). In the disuse group, however, the elastic modulus differences in the anterior posterior regions reduced to 1.2GPa from 2.6GPa in the control group, and increased in the medial region to 2.7GPa from 0.2GPa. It is suggested that material property of bone may be strongly influenced by the overall strain magnitude in the healthy skeleton. Such pattern was compromised in disuse osteopenia, suggesting that the remodeling in distribution of micro-nano elastic moduli among different regions may serve as a predictor for early stage of osteopenia. In the second part of the study, to obtain data in all directions, the bone was cut in - a) transverse plane (axial), b) coronal plane (circumferential), and c) sagittal plane (radial). Mechanical properties, such as elastic

modulus (E) and hardness, were calculated by nanoindentation on the periosteal and endosteal surfaces over the lateral region of the bone samples. Results showed -1) an anisotropic bone structure with axial and radial directions with the highest and the lowest E values, respectively, on both periosteum and medullary endosteum; and 2) a statistically significant difference between the control and the disuse group on the E values of the endosteum in the radial and circumferential directions. It is suggested that the functional disuse weakened the mechanical properties of the endosteum but not the periosteum. These findings have high clinical significance for the study of drug designing and mechanotransduction pathways. It is also accrued that the nano-mechanical properties in the axial orientation were not affected from the one month of functional disuse, pointing geometrical anisotropy in the remodeling processes.

Dedication Page

I would like to dedicate this thesis to my parents who have been my constant source of power and inspiration. If it wasn't for them I would have never been able to focus on my research and stand where I am today. It was there constant motivation that kept me going.

Table of Contents

List of Figures

Figure caption

List of Tables

List of Abbreviations

DXA- Dual Energy X Ray Absorptiometry

QCT- Quantitative Computed Tomography

pQCT- peripheral Quantitative Computed Tomography

HLS- Hind Limb Suspension

AFM- Atomic Force Microscopy

GPa- Giga pascal

LI- Laminarity Index

AFM- Atomic Force Microscopy

FEA- Finite Element Analysis

Acknowledgments

I would like to acknowledge my advisor, professor Yi-Xian Qin who is an excellent mentor. The weekly feedback and help I received from him in every lab meeting made this project go further. His constant guidance and patient listening to my doubts as well as spending time with me on my problems have been vital for this thesis.

I would like to acknowledge professor Wei Lin who was also a constant guide to this thesis project. His feedback in the lab meetings has been a crucial part of this thesis. His insight into the project and excellent questions made the thought process run a step ahead and motivated me to work harder.

I would like to acknowledge professor Balaji Sitharaman who is not only an excellent mentor but also a great teacher. His constant support in the project and classes headed me in the right direction.

And this thesis would not be possible without my lab team who are one of the most important reasons that this work was completed. I would like to specifically mention Minyi Hu, Liangjun Lin, Jesse Muir, Tony Zhang, Jian Jiao, Lily Huang and Xiaofei Li. Their constant support, help and feedback made this work go through till the end.

Chapter 1: Introduction

BONE TISSUE

Bone is composed of cells, minerals and elastic collagen fibers. The bone cells are embedded in the organic matrix of the bone. Bone has mainly four types of cells- osteoblasts, osteoclasts and osteocytes, lining cells and their progenitor forms. Even after growing to their maximum size bones keep on remodeling themselves by destroying old bone and creating new one instead of it. Osteoblasts are bone cells responsible for bone formation and osteoclasts are bone cells being responsible for bone absorption ((Burger and Klein-Nulend, 1999). The bone matrix is composed of organic and inorganic parts. Organic part is the collagen fibers and the inorganic part is mineral content in the form of carbonated hydroxyapatite ((Legros et al., 1987)). The hard mineral content and collagen fibers together sustain the loads. Below is given a cross-section of compact bone (Fig 1.1).

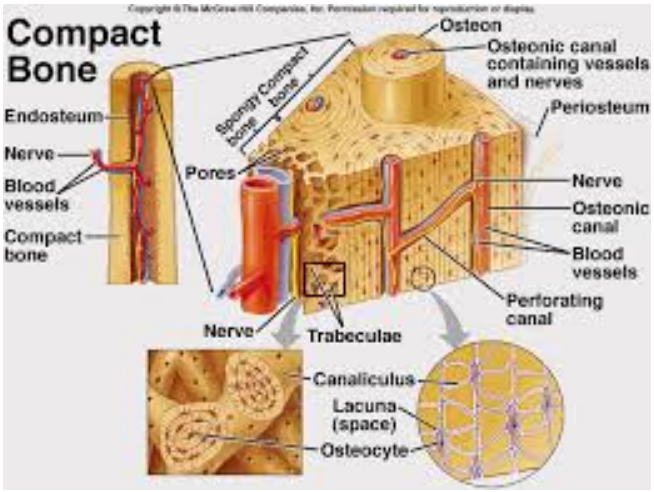

Fig 1.1 Cross-section of a bone showing the periosteum,endosteum and the osteon structure.

Bone has a complex hierarchical structure (Currey, 2003; Rho et al., 1998). The mechanical competence of bone at the micro length scales is due to a combination of collagen fibrils and crystalline mineral hydroxyapatite (Weiner et al., 1999). In a single bone, transverse cross-section range of mechanical properties can be observed (Courtland et al., 2008; Donnelly et al., 2010; Lewis and Nyman, 2008). The periosteal side of the bone is the bone forming layer (Clarke, 2008; Ved and Haller, 2002). The periosteum consists two separate layers, the outer fibrous layer and the inner cellular layers. While the outer layer is highly vascularized, the inner layer has a high osteogenic potential (Dwek, 2010). However, it is the endosteal side of bone, which is the resorption layer of the bone.

BONE – USE AND DISUSE

Shear forces imparted by bone fluid in the canaliculi, is one of the possible mechanotransduction pathways inside the osteocytes, which further leads to bone formation (Burger and Klein-Nulend, 1999; Huang and Ogawa, 2010; Knothe Tate et al., 1998; Qin et al., 2010; Qin et al., 1998; Reich et al., 1990; Rubin et al., 1997; Turner et al., 1994; Weinbaum et al., 1994). Previous research showed that cyclical loading increased the mechanical properties of bone, and that absence of loading caused loss of mechanical strength in bone (Burger and Klein-Nulend, 1999; Donaldson Cl Fau - Hulley et al., 1970; Huang and Ogawa, 2013; Manske et al., 2009; Qin et al., 1998; Rubin Ct Fau - Lanyon and Lanyon, 1987; van der Meulen et al., 2006; Wallace et al., 2009; Wolf, 1995).

It has been further shown that osteoporotic conditions cause an increase in remodeling rate, which causes an increase in the endosteal resorption and then a decrease in cortical thickness and a loss of structural index (Seeman, 2003; Szulc et al., 2006). Previous research also showed that

unloading or disuse increased endosteal bone resorption, but loading caused an increase in periosteal bone formation and mineralization (LaMothe et al., 2005). It is further shown that exercise and mechanical loading increased periosteal perimeter and periosteal mineral apposition rate in mice tibiae (Kodama et al., 2000).

Victims of functional loading can be astronauts on long- term space flights, patients of prolonged bed rest or of paralysis ((Lau and Guo, 2011)). Such conditions lead to significant reduction of mineral, alteration of architecture and severe loss of mechanical strength.

CLINICAL NEED AND CURRENT CLINICAL DIAGNOSIS METHODS

For an effective treatment of osteoporosis or mechanical disintegration of bone tissue, the first clinical need is to have an early diagnosis. In this step indicative parameters are to be found which change due to disuse conditions. Dual Energy X-ray absorptiometry (DXA) uses low-level energy X-ray to determine the material property of bone, but does not provide the micro-mechanical properties (McPherson et al., 2014; Weryha et al., 1991). To assess bone mineral density through T and Z scores obtained from DXA is the main clinical measurement for osteopenia and osteoporosis (Gilsanz, 1998; Lata and Elliott, 2007; Ryan et al., 2011). Though there are alternative methods, e.g., use of ultrasound (Hakulinen et al., 2004; Kotha et al., 2008; Lin et al., 2014; Qin et al., 2013) and quantitative computed tomography (QCT) and peripheral QCT (pQCT) techniques (Engelke et al., 2013; Xing et al., 2003) to determine bone strength and micro-architecture.

NANOINDENTATION

Nanoindentation is an indentation procedure to calculate sample hardness and elastic modulus.

Nanoindenter Tip

Some of the widely used indenter tips used are-

1. 3-Sided Pyramidal Tips
    a. Berkovich: This is one of the most widely used nanoindentation tip which is used. It has a diamond tip. The half angle is 65.35 degrees, the aspect ratio of the tip is 1:8 and its radius of curvature is approximately 150nm. This is also the tip used in this study.
    b. 90 degree (Cube corner tip)
2. Conospherical Tips
    a. Imaging tips
    b. Non-Imaging tips
3. Specialty Tips
    a. Vickers
    b. Knoop
    c. Flat Ended
    d. Wedge

Theory of Calculating Elastic Modulus from Indentation

For a Berkovich tip-

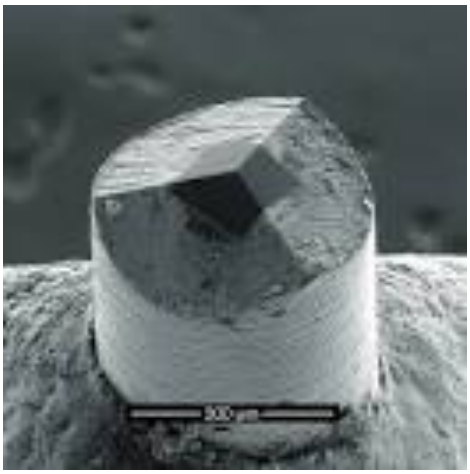

Fig 1.2 Pyramidal Berkovich tip of a nanoindenter

$A = 24.5 * h_c^2$

Where A is the projected contact area; h_c is the contact height

$$A = \left(\frac{\pi}{4}\right) * \left(\frac{S}{\mathrm{Er}}\right)^2$$

Where E_r is the reduced Young's modulus and S is the stiffness, which is calculated form the initial unloading contact stiffness during the indentation.

$$\frac{1}{\mathrm{Er}} = \left(\frac{1 - \square^2}{\mathrm{E}}\right)\mathrm{specimen} \quad + \quad \left(\frac{1 - \square^2}{\mathrm{E}}\right)\mathrm{indenter}$$

where E and ν are the elastic modulus and Poisson ration of the specimen and indenter respectively.

$$H = \frac{Pmax}{A}$$

Where H is the hardness, P_{max} is the maximum indentation force and A is the resultant projected contact area at that load.

HYPOTHESIS AND SPECIFIC AIMS

AIM 1-To assess the effect of regional strain distribution on spatial distribution of micro-mechanical modulus in a healthy bone and to investigate remodeling in the spatial distribution from osteopenia set in by functional disuse

HYPOTHESIS- Micro mechanical modulus distribution should be dependent upon the micro strains experienced by the control tibia bone. Regions of higher micro-strains should have higher micro-mechanical moduli as compared to regions of lower micro-strains. In the disuse bone however the correlation between micro-strains and micro mechanical moduli should diminish.

AIM 2-To assess periosteal and endosteal anisotropy in a healthy bone and to investigate remodeling in anisotropy from osteopenia set in by functional disuse

HYPOTHESIS- In the control samples micro-mechanical moduli anisotropy ought to be present at both the periosteal and endosteal sides of the bone in the lateral region. However the anisotropy will be absent in the functional disuse group.

Chapter 2: Spatial Distribution and Remodeling of Elastic Modulus of Bone in Micro Regime as Prediction of Early Stage Osteopenia

INTRODUCTION

Bones, the load bearing organ, bear the weight of the human body and also bear the loads applied on it during locomotion (Pekka, 2007). As a living tissue, skeleton continuously keeps on modeling and remodeling itself (Burger and Klein-Nulend, 1999). It is demonstrated that loading affects the mechanical properties of bone, while the absence of loading causes loss of its mechanical strength (Burger and Klein-Nulend, 1999; Huang and Ogawa, 2013; Qin et al., 1998; Wolf, 1995). It is proposed that osteocytes are responsible for sensing the mechanical loads (Burger and Klein-Nulend, 1999; Kelly and Bronk, 1990; Qin et al., 2010; Weinbaum et al., 1994). Shear forces by induced bone fluid on the osteocytes leads to formation of more bone (Burger and Klein-Nulend, 1999; Knothe Tate et al., 1998; Qin et al., 2010; Reich et al., 1990; Rubin et al., 1997; Weinbaum et al., 1994).

Work conducted in the past shows correlation between bone tissue strain and mechanical properties of bone(Carter, 1982; Frost, 1983; Lanyon, 1987; Main et al., 2010). Conditions such as osteoporosis adversely affect bone's mechanical strength. Previous work so far has been focused primarily on the overall strength of bone and how loading or disuse affects its mass and strength. Prediction of the risk of fracture from bone mechanical properties and density values has been the key focus of a lot of studies on osteoporosis. Dual Energy X-ray absorptiometry (DXA) uses low-level energy X-ray to determine the material property of bone, but does not provide the micro-mechanical properties (McPherson et al., 2014; Weryha et al., 1991). To assess bone mineral density through T and Z scores obtained from DXA is the main clinical

measurement for osteopenia and osteoporosis (Gilsanz, 1998; Lata and Elliott, 2007; Ryan et al., 2011). Though there are alternative methods, e.g., use of ultrasound (Hakulinen et al., 2004; Kotha et al., 2008; Lin et al., 2014; Qin et al., 2013) and quantitative computed tomography (QCT) and peripheral QCT (pQCT) techniques (Engelke et al., 2013; Xing et al., 2003) to determine bone strength and micro-architecture.

Nanoindentation allows measurement of mechanical properties such as elastic moduli and hardness at a micro and nano scale resolution level (Angker et al., 2005; Ebenstein and Pruitt, 2004; Fan et al., 2002). Nanoindentation has been recently used in a lot of studies to measure hydrated mouse bone mechanical properties(Pathak et al., 2011a), lamellar level bone mechanical properties and sub micron mechanical properties(Pathak et al., 2012b; Silva et al., 2004). In recent years studies have been undertaken to investigate regional microstructural properties of bone where relations between regional mineralization density and col`lagen fiber orientation were correlated(Goldman et al., 2005). Another previous study has shown that cortical bone is significantly inhomogeneity dependent on it's mechanical strain. For example, using an avian ulnae model, there were significant differences between difference bone regions in the cross sections, in which mean laminarity indexs (LI) were varied between subadult (40.0% +/- 10.7%) and adult (50.9% +/- 10.4%) bones, and their related bone strain(Skedros and Hunt, 2004), suggesting that regional microstructure and associated mechanical strength may strongly influence by local mechanical loading(McLeod et al., 1998; Qin et al., 1998; Skedros et al., 2004).

Though some work has been conducted to measure micro-mechanical properties of the bone (Angker et al., 2005; Fan et al., 2002; Hengsberger et al., 2002; Hoffler et al., 2005), a complete picture of how these properties spatially differ in various regions of a bone section and how they

vary from the periosteal to the endosteal side of bone has not been formulated, particularly its dependence on the local mechanical strain. Moreover, effect of functional disuse of bone on the spatial distribution of such micro-mechanical moduli has not been evaluated. Victims of functional disuse can be astronauts on long-term space flights, patients of prolonged bed rest or of paralysis and traumatic brain injury (Lau and Guo, 2011).

The objectives of this study were to evaluate the micro-nano mechanical elastic modulus differences from periosteum to endosteum in rat tibia mid shafts, and to correlate them to its associated strain distribution. In addition, the effect of disuse on the spatial distribution of the micro-nano elastic modulus was evaluated. The hypothesis of the study was that regional strain distribution will determine the regional micro-mechanical moduli distribution in the cortical tibia bone cross-section Regions of high strain would have a higher micro mechanical modulus as compared to regions of low strain which would have a lower micro mechanical modulus. But such a correlation between strain and micro mechanical moduli would not be present in the cross-sections of the functional disuse groups.

METHODS

Bone samples from left tibia were obtained from 5-month old virgin female Sprague Dawley rats, including 1) baseline control (n=9), and 2) hindlimb suspended (HLS) (4 weeks, n=9) (Hu et al., 2012). The animal study was previously approved by the Stony Brook University IACUC.

Sample Preparation

After a cross-sectional cut and clearing of the bone marrow using a water jet, 2mm in longitudinal length segments at the midshaft were cut from the transverse plane using a diamond

wheel saw (South Bay technology Inc., MODEL 650, Clemente, California, USA) under constant water cooling.

Embedding and Polishing

The bone samples were stored in ethanol of subsequent higher concentrations of 70%, 80%, 90% and then 100% each for 2 days for complete drying. Subsequently they were embedded in epoxy resin and let to cure for a day (Fig 2.1). For exposing the surface of bone, the embedded samples were first polished with silicon carbide papers (Buehler-Carbimet, Illinois, USA) (Fig 2.2) of grit numbers 320, 600, 1200, 2400, 4000 mounted on a Buehler grinder Power pro 3000^{TM}(Illinois, USA) in the respective sequential order. Finally the samples were polished by Polycrystalline Diamond Suspensions (Buehler MetaDi^{TM}Supreme) of roughness 3μm, 1μm, 0.25μm and finally by 0.05μm in the given descending order.

Fig 2.1 Bone samples prepared after embedding in epoxy

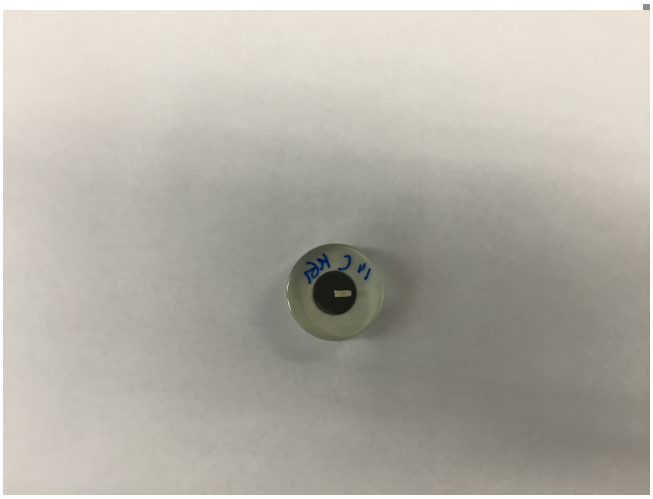

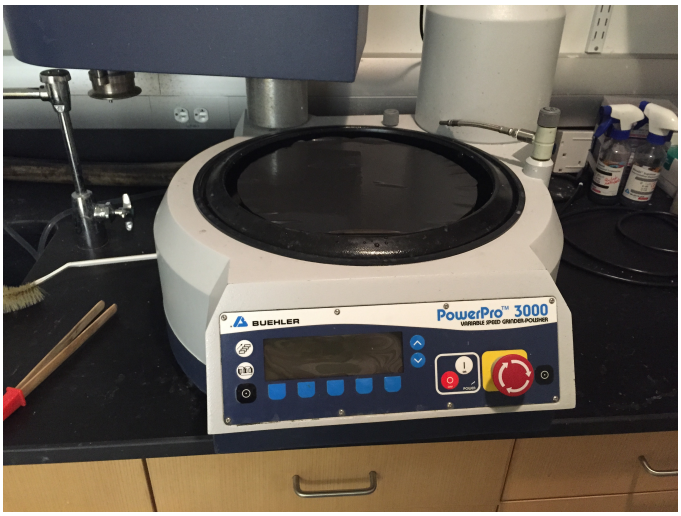

Fig 2.2 Buehler machine used for grinding of samples under constant water irrigation

Nanoindentation

Fig 2.3 Hysitron Triboindenter TI-950, used for nanoindentation

The distribution of mechanical properties of bone such as elastic modulus and hardness were measured on a micro scale in the z or axial directions by Nanoindentation (Hysitron Triboindenter TI-950, Minneapolis, Minnesota) (Fig 2.3) at precise locations. Tip of the nanoindenter was a diamond Berkovich tip. Atomic Force Microscopy (AFM) (TED PILLA.

INC, USA) specimen disks of 15mm diameter (Fig 2.4) were stuck to the base of the samples by cyanoacrylate and then the samples were loaded on the magnetic base of the triboindenter. It was

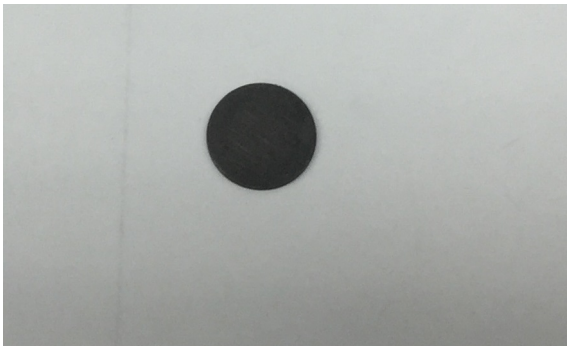

Fig 2.4 AFM disk used to attach samples to magnetic base of nanoindenter

made sure that the samples with the discs at the bottom were attached firmly and the specimens do not rotate on the magnetic base. For consistency in all the samples, indents were made near

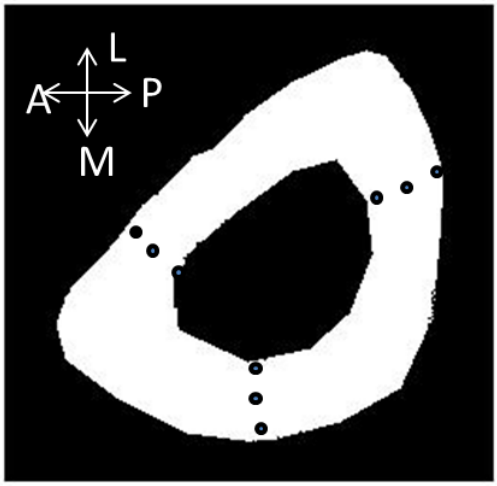

Fig 2.5 Image displaying the indents, which are shown by the black dots, on the anterior, posterior and medial regions near the periosteal, endosteal and also in the middle of the axial section of the rat tibia.

the periosteal side, near the middle and also near the endosteal side of the bone in the anterior, posterior and medial regions of the bone as shown in Figure 2.5.

The points of indentation on the bone were chosen after viewing the cross-section under the imaging system of the triboindenter, which comprised of an objective of magnification 10X and an end zooming lens of magnification 2X. No need of further magnification was felt to select points for indentation.

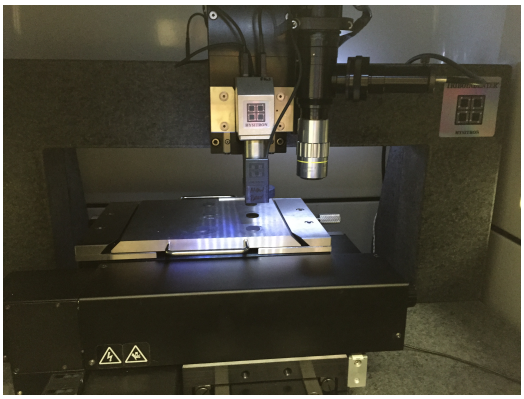

Fig 2.6 Nanoindenter and the microscope system of the triboindenter

The tip area function was calibrated from indentation analysis on fused quartz, and drift rates in the system were measured prior to each indentation using standard indentation testing procedures. A preload of 2μN was used while indentation. The indentation consisted of a 10 seconds loading period at a constant loading rate of 100μN/s. A constant load segment at the peak load of 1000μN followed this for a time of 30 seconds. In the end the tip was retracted in the unloading segment for another 10 seconds at a constant unloading rate of 100μN/s. The total

indentation time was 50 seconds (Figure 2.7).

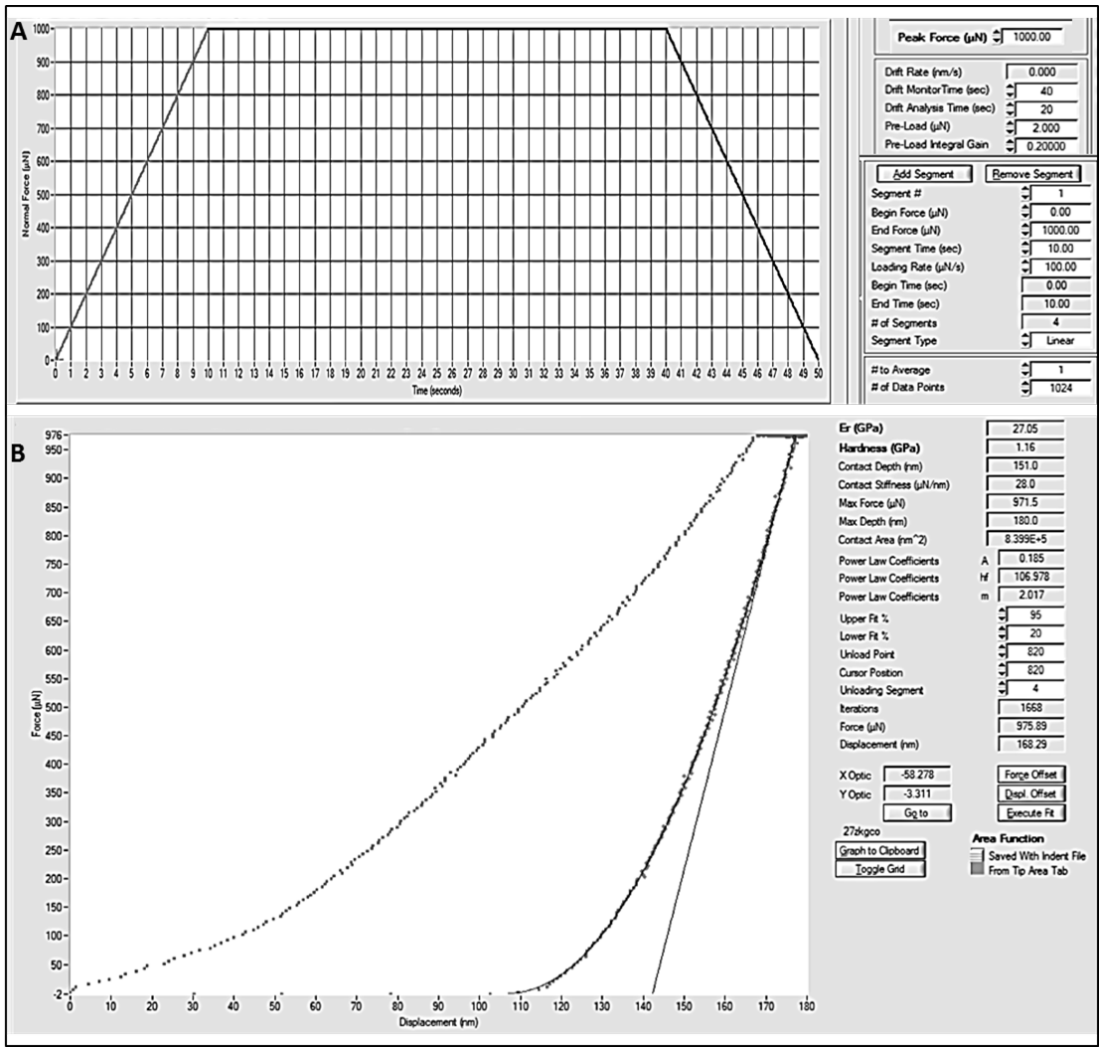

Fig 2.7.A. Displacement –time curve of the load function being used for indentation of samples. B. Force displacement curve of the Berkovich tip of the nanoindenter into the sample. The slope of the best- fit line is used to calculate the elastic modulus from the nanoindentation raw data.

The elastic response was calculated from the 20–90% portion of the unloading curve. Elastic modulus was calculated assuming an elastic response during unloading and using Oliver Pharr Method(Hoc et al., 2006). Indentation Load vs. Displacement curves are given in the supplementary figures.

Mechanical Loading and Strain Gauge Measurement

Three additional control rats were sacrificed and their left hindlimbs were removed from the hip joint. With the soft tissues and muscles still attached the hindlimbs were axially loaded, from knee to the foot joint on the Bose Electroforce machine (BOSE, Inc. Minneapolis, Minnesota) (Fig 2.8). Strain gauges were attached to the mid-shaft tibia bone at the anterior, posterior and medial sides of the bone in a rosette pattern for measurement of strain induced by the loading. Peak to peak strains at three strain gauge sites were measured around the mid-tibia (National Instruments Strain acquisition box). Labview was used to control the operation of measurement of strains. The hindlimbs were loaded with a sinusoidal load function with peak magnitudes ranging from 6-10N at 1Hz frequency in load control mode. A 1Hz frequency was chosen to mimic a normal rat's walking gait frequency and low forces were investigated to produce strains in accordance with previous research (Hsieh et al., 1999; Torcasio et al., 2012). The Bose Machine recorded displacement and the load on the bone, while strains produced (peak to peak) were measured on the LabView software via the NI (National Instruments) Strain Acquisition Box.

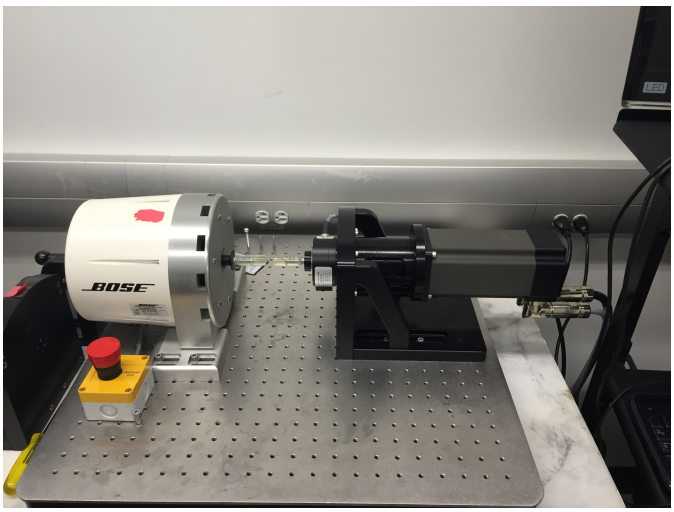

Fig 2.8 Bose Electroforce machine used for axial loading of rat tibia

μCT scanning

The left tibias were later removed from the rest of the hindlimbs by dislocating the tibia at the knee and feet joint. All the soft tissues were removed and the bone was cleaned. The strain gauges were not disturbed at this step and still left attached to the bone. The whole bone was then scanned in μCT scanner (SCANCO Inc.) with 36μm resolution. Image slices of the bones having the three strain gauges attached were chosen for further analysis of strain distribution.

MATLAB Image Processing

Slice with all the three strain gauges attached in a rosette pattern were chosen for MATLAB (version 2013a) image processing and further analysis. The corners of the bone slice were smoothened and some unnecessary external features were cropped out (such as wires) from the bone slice by ROI poly method in MATLAB. Coordinates of the image pixel representing the bone just next to the middle of the strain gauge attached was given the strain value (peak to peak) as measured by the strain gauge. Using linear beam theory MATLAB codes were built to find planar strain distribution across the whole bone slice (Serra-Hsu et al., 2011).

Statistical Analysis

The data of Nanoindentation from the Tribo Scan software of Hysitron Triboindenter and of the strain values from National Instruments Strain Acquisition Box were exported into Microsoft Excel (Microsoft Excel 2011, version 14.0.0). Two tailed Student's t-test was performed when the control and experimental groups were compared and when the periosteal elastic moduli values were compared with endosteal elastic moduli values. However one way ANOVA test was

performed for comparing the elastic moduli of all the three anterior, posterior and medial regions together in both the control and experimental groups. IBM statistical software SPSS 22.0 was used to conduct for statistical analysis. The significance level was set at 0.05 for both the student t-test and one way ANOVA tests.

RESULTS

Nanoindentation

A total of 6 areas of interest were investigated for each segment. The mean of the periosteal, middle and endosteal elastic moduli was regarded as the mean indentation value of the region. The indentation values at the various regions are in Table1.

	ANTERIOR		POSTERIOR		MEDIAL	
	PERIOSTEUM (In GPa)	ENDOSTEUM (In GPa)	PERIOSTEUM (In GPa)	ENDOSTEUM (In GPa)	PERIOSTEUM (In GPa)	ENDOSTEUM (In GPa)
CONTROL	28.81±2.78	25.58±2.99	27.15±2.65	26.62±3.97	28.65±2.25	28.16±3.19
EXPERIMENTAL	27.13±3.15	26.52±4.41	29.13±3.23	25.17±4.3	28.45±3.35	27.15±3.21

The p values between the control and experimental group were: anterior, p=0.04; posterior, p= 0.28; medial, p=0.13. It was observed that the elastic modulus difference from periosteum to endosteum was much higher in the anterior and posterior regions (2.6GPa) than the medial

region (0.2GPa), in the control group (Fig.3).

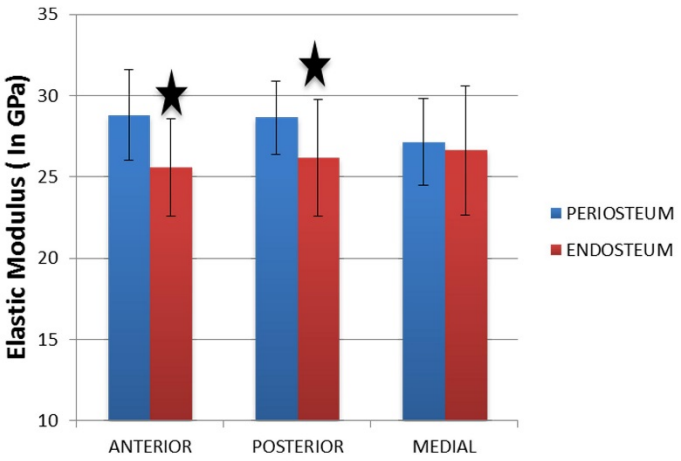

Fig 2.9 Elastic moduli of periosteal and endosteal sides of each region of bone investigated in control group shown as mean and standard deviations. A * sign on the endosteum represents significant difference from the periosteum.

In the same group the periosteum and endosteum were significantly different (in terms of elastic moduli) in the anterior and posterior regions- $p<0.001$ and $p<0.001$ respectively. In the medial region the difference of elastic moduli between periosteal and endosteal side was not statistically significant ($p=0.41$).

In the disuse group, however, the elastic modulus difference in the anterior posterior direction was reduced to 1.2GPa, and increased in the medial direction, 2.7GPa.

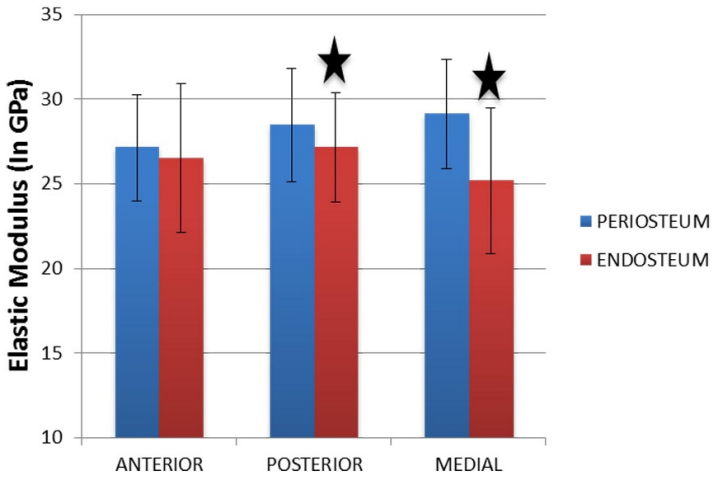

Fig 2.10 Elastic moduli of periosteal and endosteal sides of each region of bone investigated in experimental group shown as mean and standard deviations. A * sign on the endosteum represents significant difference from the periosteum.

The periosteum and endosteum were not statistically different in the anterior region- p= 0.4. However in the posterior and medial regions the difference between the periosteal and endosteal side was statistically significant (p=0.01 and p<0.001 respectively).

Strain Gauge Measurement

In the control group, strain (peak to peak) distribution in mid tibia shaft further showed similar higher strain difference in the anterior-posterior (45με) but reduced to 5με in the lateral medial direction.

μCT Images

The three tibias obtained were scanned in μCT scanner with 36 μm resolution. Three different slices, which best represented the three strain gauges on the three different bones were chosen for strain analysis in MATLAB.

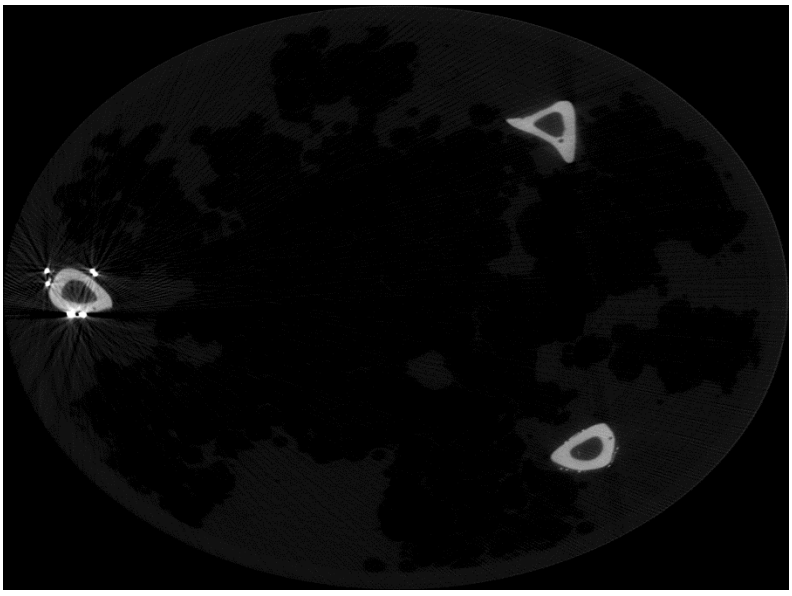

Fig 2.11 Micro CT scan of the three rat tibias and also showing the strain gauges attached on the surface

MATLAB Image Processing and Strain Analysis

After processing the image through ROI poly, the bone section was converted into a polygon in the shape of the section itself. Using linear beam theory the MATLAB codes built gave a strain distribution across the tibia scan. One such strain distribution is shown in Figure 5.

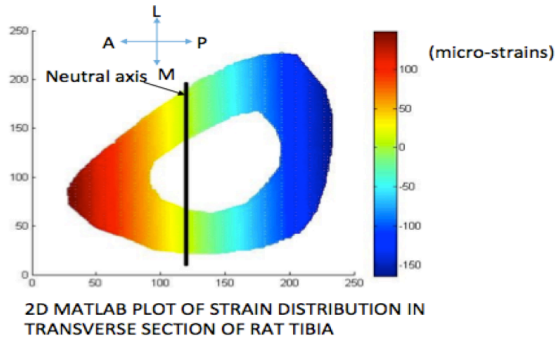

Fig 2.12 2D Matlab plot of planar strain distribution in transverse section of rat tibia due to loading. Red shows positive strain values or tension, whereas blue shows negative strain values or compression inside the bone.

The strain distribution clearly showed that the anterior side of the bone was under tension, while the posterior region was under compression. The average tension to compression ratio was approximately 1:1.25. This showed that the tibia mid-diaphysis is under higher compression than tension. This was in accordance with previous studies done on rat tibia mid- diaphysis (Patel et al., 2014). The neutral axis obtained was roughly parallel to the posterior side of the bone in all the three sections investigated.

DISCUSSION

Previous research showed that the fluid flow in the canaliculi causes shear stresses on the osteocytes, which serve as the beginning of the mechano-sensing pathway (Gross D Fau - Williams and Williams, 1982; Huang and Ogawa, 2013; Qin et al., 2010; Qin et al., 1998; Rubin Ct Fau - Lanyon and Lanyon, 1987; Zeng et al., 1994). The bone fluid flow remodeling theory

brought a high interest in the investigation of what causes the fluid flow and what are its effects. Research has indicated that activities from daily life, causing bone strain, can induce bone fluid flow (Burger and Klein-Nulend, 1999; Gross D Fau - Williams and Williams, 1982; Hu et al., 2012; Qin et al., 2010; Reich et al., 1990; Serra-Hsu et al., 2011; Weinbaum et al., 1994; Wolf, 1995) and can cause a bone fluid flow movement. Research was also conducted to identify the nature of the bone fluid flow and the effect of magnitude, frequency of flow on bone formation(Hu et al., 2012; Hu M, 2014; Qin et al., 2003; Qin et al., 2010). More recently the focus has gradually shifted form macro to the micro strains in various regions of a bone section and the mechanical properties as well as mineralization density and collagen fiber orientation of each region of a bone section and showing stark differences from one region to another(Bonney et al., 2011; Goldman et al., 2005; Hammond et al., 2014; Ramasamy and Akkus, 2007). Micro level mechanical as well as material properties have increased our understanding of bone remodeling and through the advent of nanoindentaiton now it is possible to study bone even on sub micron and nano scales. Variation of mechanical parameters within a region of bone from periosteum to endosteum and the effect of functional disuse on the same was the key objective of this study.

This study was focused on the analysis of possible correlation between the strain and the micro-nano level mechanical properties in different regions of a bone section. The mean insignificant p values between all the three regions investigated in a healthy or control bone showed that the modeling and remodeling activity was similar in all the three regions and were not different from an elastic moduli point of view on a sub-millimeter or still a macro level. While there were no significant difference between the control and experimental groups for averaged mechanical properties in all the regions, strong correlation between strain and elastic modulus against

periosteum and endosteum was observed in the control group. However, the spatial distribution of the elastic modulus difference pattern in the disuse experimental group was not same as the control group.

Significant differences between the periosteum and endosteum (in terms of strength) in the anterior and posterior regions and insignificant differences in the medial region suggest that the remodeling mechanism inside the bone can sense not only total strain but also the difference in strain experienced by the periosteal and endosteal sides of bone. The square of correlation coefficient R^2 >0.95 was obtained when all the strain differences in the anterior, medial and posterior regions of the three additional control rats were plotted against the average elastic moduli differences in the same respective regions (Fig. 6).

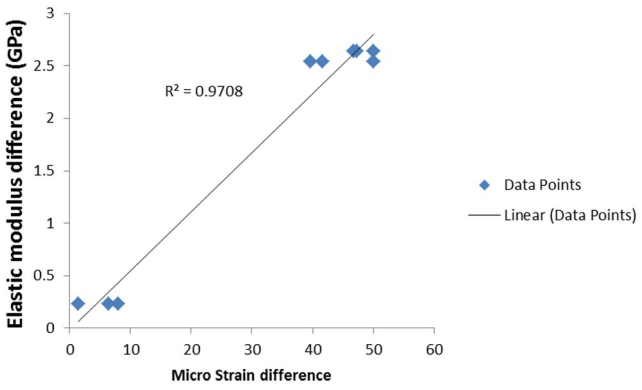

Fig 2.13 Graph showing high correlation between elastic modulus difference and micro strain difference in the control group for the anterior, posterior and medial regions of rat bone. The solid line represents the linear fit between the data points, which gives $R^2 = 0.9708$.

Wolff's law which was further improved upon in Frost's law, states that due to loading bone adapts itself to become stronger (Frost, 1994). However an adaptation to micro strain differences in such small distances has not been discussed so far. Such an anisotropic remodeling points out to the extreme sensitivity of the mechano-sensing and transduction mechanism.

Hence our hypothesis that strains present inside the bone cross section determine the modulus of that region is true as high a strain difference also causes a high micro-mechanical modulus

difference at the anterior and posterior regions but a lower micro-strain difference in the medial region caused a lower micro mechanical moduli difference in the medial region. In the disuse group however we see a change in the micro-mechanical moduli difference trends, suggesting that remodeling due to functional disuse is set in.

The difference in elastic modulus distribution between a healthy bone and a one-month functional disuse bone suggests that this could serve as a predictor for the onset of osteopenia. But such change in mechanical modulus distributions within the bone will be completely unobservable in DXA as it assesses the mean mechanical properties on which no effect has taken place from one month of functional disuse. The studying of sub-micro mechanical differences will take into account mechanical properties as well as structural integrity or shape of the bone. It is critical to study here that nano-indentation was performed after the sacrifice of rats. A need for a tool to assess the same properties in a non-invasive manner is required. This can be done through the use of ultrasound by which such properties can be investigated without invading the human body. However the ultrasound transducers have to be powerful so as to measure the exact modulus difference within each region.

Recent study has also demonstrated that microindentation on the bone surface can cause micro-fractures and the analysis of these may be able to correlate with the overall mechanical property of bone tissue. In this method a reference point indentation instrument was used which loads the bone surface at a particular load and frequency and measures the surface mechanical properties(Diez-Perez et al., 2010; Gallant et al., 2013; Granke et al., 2014).

CONCLUSION

The study shows that bones can sense spatial strain distribution in micro scales and change its micro-mechanical properties accordingly in the different regions. Initial damage from functional disuse is on the spatial distribution of micro-nano elastic modulus of the various regions of bone, though the average macro strength might be similar to the control group. Geometrical anisotropy in the mechano-sensing and transduction pathways of the bone is highlighted.

Chapter 3: Damage from Functional Disuse Begins at Endosteum in Radial and Circumferential Orientations: A Nanoindentation Study on Lateral Region of Cortical Mid-shaft of Rat Tibia

INTRODUCTION

Shear forces imparted by bone fluid in the canaliculi, is one of the possible mechanotransduction pathways inside the osteocytes, which further leads to bone formation (Burger and Klein-Nulend, 1999; Huang and Ogawa, 2010; Knothe Tate et al., 1998; Qin et al., 2010; Qin et al., 1998; Reich et al., 1990; Rubin et al., 1997; Turner et al., 1994; Weinbaum et al., 1994). Previous research showed that cyclical loading increased the mechanical properties of

bone, and that absence of loading caused loss of mechanical strength in bone (Burger and Klein-Nulend, 1999; Donaldson Cl Fau - Hulley et al., 1970; Huang and Ogawa, 2013; Manske et al., 2009; Qin et al., 1998; Rubin Ct Fau - Lanyon and Lanyon, 1987; van der Meulen et al., 2006; Wallace et al., 2009; Wolf, 1995). Various indicative parameters of bone health include elastic modulus, hardness, mineralization density, cross-sectional area, bone anisotropy, structural modulus index, collagen fiber density and orientation. Past work has shown that disuse decreased bone geometrical properties and mineralization (Gross and Rubin, 1995; Hoffler et al., 2005; Kaneps et al., 1997). Healthy bones, especially the load-bearing bones, have a high degree of anisotropy. The weight-bearing bones usually have a higher strength in the longitudinal direction so that they can sustain the compressive loads being applied during walking, running and other activities (Hoffmeister et al., 2000).

To assess the detrimental effects of disuse, in the present study, the micro-anisotrpy of the load bearing tibial bone was investigated. Bone has a complex hierarchical structure (Currey, 2003; Rho et al., 1998). The mechanical competence of bone at the micro length scales is due to a combination of collagen fibrils and crystalline mineral hydroxyapatite (Weiner et al., 1999). In a single bone, transverse cross-section range of mechanical properties can be observed (Courtland et al., 2008; Donnelly et al., 2010; Lewis and Nyman, 2008). The periosteal side of the bone is the bone forming layer (Clarke, 2008; Ved and Haller, 2002). The periosteum consists two separate layers, the outer fibrous layer and the inner cellular layers. While the outer layer is highly vascularized, the inner layer has a high osteogenic potential (Dwek, 2010). However, it is the endosteal side of bone, which is the resorption layer of the bone. It has been shown that osteoporotic conditions cause an increase in remodeling rate, which causes an increase in the endosteal resorption and then a decrease in cortical thickness and a loss of

structural index (Seeman, 2003; Szulc et al., 2006). Previous research also showed that unloading or disuse increased endosteal bone resorption, but loading caused an increase in periosteal bone formation and mineralization (LaMothe et al., 2005). It is further shown that exercise and mechanical loading increased periosteal perimeter and periosteal mineral apposition rate in mice tibiae (Kodama et al., 2000). However, the results of bone remodeling on the mechanical properties in the three orthogonal orientations- axial, circumferential and radial orientations remain to be worked out.

Nanoindentation is considered an important tool for the investigation of mechanical properties, such as elastic moduli and hardness, possibly at the micro and nano levels (Angker et al., 2005; Ebenstein and Pruitt, 2004; Fan et al., 2002; Hoffler et al., 2005; Imbert et al., 2011; Lewis and Nyman, 2008; Pathak et al., 2012a). Earlier work has shown that bone has a definite anisotropy in its mechanical properties(Fan et al., 2002; Khandaker and Ekwaro-Osire, 2013). In addition, studies have been undertaken to measure the anisotropy of single primary and secondary osteons in the cortical bone using nanoindentation techniques (Carnelli et al., 2013; Faingold et al., 2012; Franzoso and Zysset, 2009; Reisinger et al., 2011). It has emerged that the cortical bone osteons have higher axial strength, which was against the twisted plywood structure of collagen fibers. Franzoso measured single secondary osteon anisotropy to emphasize the importance of length scale and the indentation depth on the mechanical properties of the osteons. However, the variation of anisotropy among the different sides of the bone, such as periosteal or endosteal, remains unaddressed so far. In addition, the effect of functional disuse on site-specific anisotropy is yet to be explored.

A rat hindlimb suspension model was used in this study for the investigation of functional disuse on site- specific anisotropy. We aimed at analyzing how functional disuse affects the

anisotropy associated with the periosteal and endosteal bone sides for the lateral region. The hypothesis for the above study was that there would be a definite anisotropy in the micro mechanical modulus at both the periosteal and endosteal sides in the control group. The stiffness at both sides of the load bearing tibia bone will be higher in the axial orientation or the main load bearing orientation. In the disuse group however due to remodeling set in by functional disuse, anisotropy in mechanical properties should not be present at the periosteal and endosteal sides, which are also the major formation and resorption zones of the bone.

MATERIALS AND METHODS

Left tibia bone samples were obtained from 5-month old female virgin Sprague Dawley rats, including 1) age matched control (n=9), and 2) hindlimb suspended (HLS) (4 weeks, n=9)(Hu et al., 2012). All indentations were carried out on the lateral side for consistency.

Sample Preparation

Cutting and clearing of Bone Marrow

For the axial orientation- 2mm thick segments were cut from the mid-shaft in the transverse plane, using a Diamond coated rotating cutter saw blade (South Bay technology Inc., MODEL 650, Clemente, California, USA) under constant water irrigation (Figure 3.1). For the circumferential orientation- 4mm thick segments were cut from the mid-shaft in the coronal plane (Figure 3.1). An indent mark was made on the lateral side.For the radial orientation- 3mm thick segments were cut from the mid-shaft in the sagittal plane (Figure 3.1). An indent mark was made on the periosteal side of the bone. Twice the number of cuts was made for the radial orientation so as to have the same number of radial orientation samples as other orientations both on the periosteal and endosteal side. The bone marrow was cleared using a water jet.

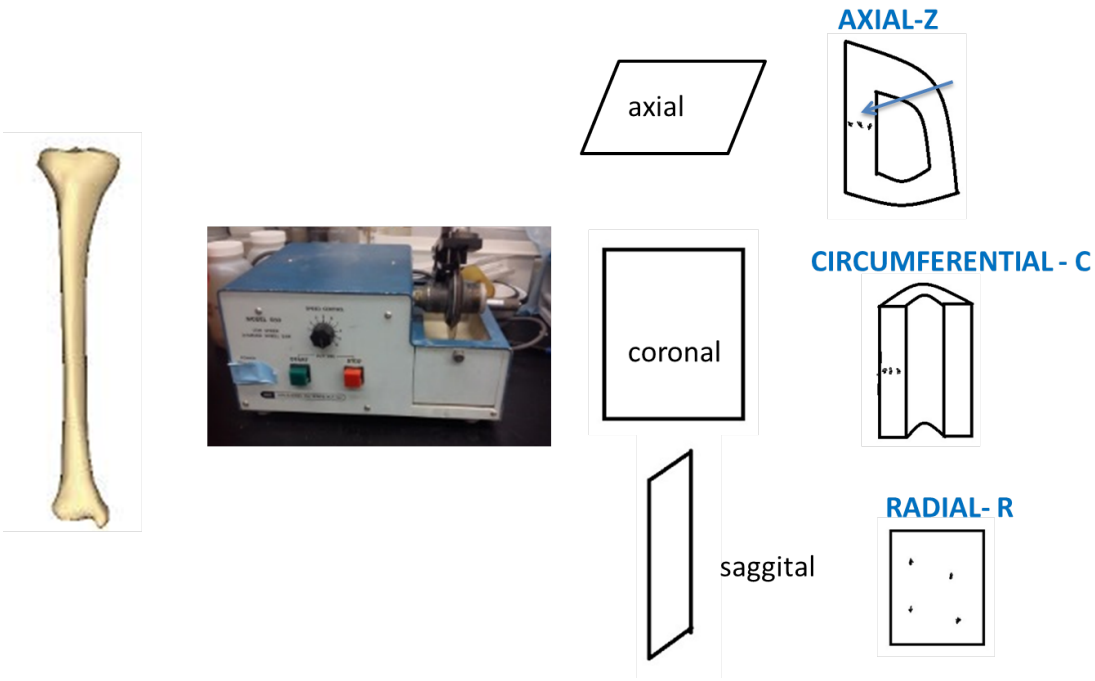

Fig 3.1 Schematic of cutting of a tibia bone in three mutually orthogonal planes i.e. the axial, coronal and sagittal planes so that the axial, circumferential and radial orientations are obtained for indenting. A diamond saw cutter blade is used for cutting of the tibia bone.

Embedding and Polishing of samples

The bone samples were stored in ethanol of subsequent higher concentrations of 70%, 80%, 90% and then 100% each for 2 days for complete drying. Afterwards the bone samples were embedded in epoxy resin and let to cure for a day. To expose the surface of bone, the embedded samples were first polished with silicon carbide papers (Buehler-Carbimet, Illinois, USA) of grit no 320, 600, 1200, 2400 and finally by 4000 on a Buehler grinder Power pro 3000^{TM} (Illinois, USA) in the respective sequential order. For the radial direction for grinding directly grit no 1200 silicon carbide was used and then subsequent higher order carbide papers were used i.e. 2400 and 4000. Great care was taken to expose just the surface and that extremely shallow grinding was obtained. Finally the samples were polished by Polycrystalline Diamond

Suspensions (Buehler MetaDi ™ Supreme) of roughness 3μm, 1μm, 0.25μm and finally by 0.05μm in the given descending order.

Nanoindentation

The distribution of mechanical properties of bone such as elastic modulus and hardness were measured on a micro scale by Nanoindentation (Hysitron Triboindenter TI-950, Minneapolis, Minnesota) at precise locations. Tip of the nanoindenter was a Berkovich tip made of diamond. AFM specimen disks of 15mm diameter were stuck to the base of the samples by cyanoacrylate and then the samples were loaded on the magnetic base of the triboindenter. It was made sure that the samples with the discs at the bottom were attached firmly and the specimens do not rotate on the magnetic base. For the axial and circumferential orientations indents were made near the periosteal side, near the middle and also near the endosteal side of the bone in the lateral region as shown in Figure 3.2. For the radial orientation for both the periosteal and endosteal sides indents were made at 4 regions, which were more than at least 100μm away as shown in Figure 3.2. The points of indentation on the bone were chosen after viewing the cross-section under the imaging system of the triboindenter, which comprised of an objective of magnification 10X and an end zooming lens of magnification 2X. No need of further magnification was felt to select points for indentation. The tip area function was calibrated from indentation analysis on fused quartz, and drift rates in the system were measured prior to each indentation using standard indentation testing procedures.

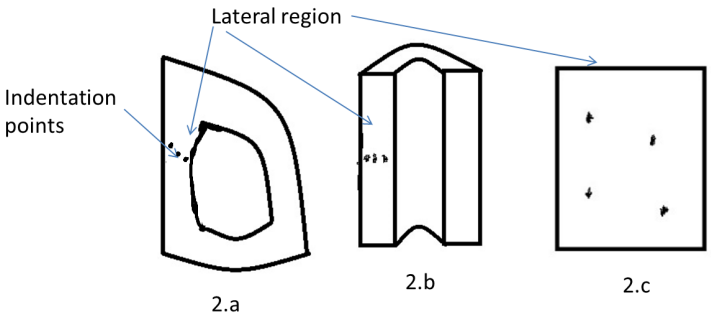

Fig 3.2 Schematic representation of the three orientations i.e. axial, circumferential and radial orientations for indenting. The black dots resemble the indentation points. All indents are performed on the lateral region of the bone.

A preload of 2μN was used while indentation. The indentation consisted of a 10 s loading period at a constant loading rate of 100μN/s. A constant load segment at the peak load of 1000μN followed this for a time of 30 s. In the end the tip was retracted in the unloading segment for another 10 s at a constant unloading rate of 100μN/s. The total indentation time was 50 s (Fig 3.3). The elastic response was calculated from the 20–90% portion of the unloading curve. Elastic modulus was calculated assuming an elastic response during unloading and using Oliver Pharr Method (Hoc et al., 2006). The values of elastic modulus and hardness were noted for each indent.

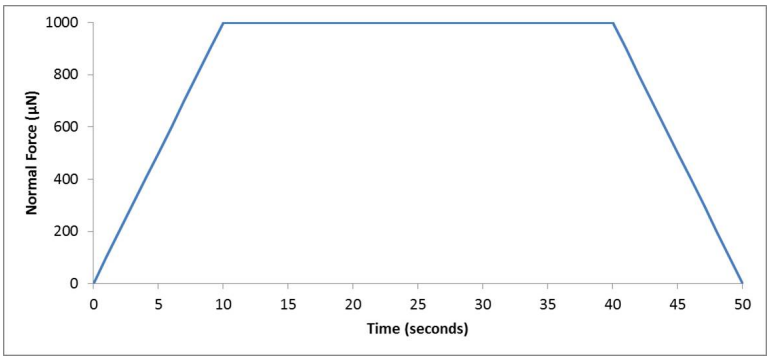

Fig 3.3 Image displaying the displacement –time curve of the load function being used for indentation of samples

Statistical Analysis

Nanoindentation data from the Tribo Scan software of Hysitron Triboindenter was exported into Microsoft Excel (Microsoft Excel 2011 for Mac, version 14.0.0). Two- tailed Unpaired Student's T.Test was performed when the control and experimental groups were compared for each of the circumferential, radial and axial orientation.One- way ANOVA test was performed for comparing the elastic moduli of all the three- axial, circumferential and radial orientations together in both the control and experimental groups. The significance level was set at 0.05 for both the T.Test and One- way ANOVA tests. All the bar charts were plotted in Excel and the graphs of loading and unloading during nanoindentation were exported from the Tribo Scan software from the Hysitron Triboindenter.

RESULTS

Bone Anisotropy

In both the control and experimental groups the Z or axial direction had the highest strength, followed by circumferential and radial directions as shown in Tables 1 and 2.

	AXIAL (GPa)	CIRCUMFERENTIAL (GPa)	RADIAL (GPa)
PERIOSTEAL	28.81±2.78	22.58±2.78	20.32±2.96
ENDOSTEAL	25.58±2.99	22.57±3.54	20.16±2.26

Table 2.1 Table showing the elastic modulus values (±standard deviations) for the control group at periosteal and endosteal regions in all the three orientations investigated.

	AXIAL (GPa)	CIRCUMFERENTIAL(GPa)	RADIAL (GPa)
PERIOSTEAL	28.49±3.35	22.62±4.47	20.52±2.69
ENDOSTEAL	27.20±3.21	21.69±3.3	17.05±3.16

Table 2.2 Table showing the elastic modulus values and (±standard deviations) for the experimental group at periosteal and endosteal regions in all the three orientations investigated.

There was a statistically significant difference among the three orientations ($p<0.05$). The anisotropy in elastic modulus could be clearly seen for the periosteal as well as endosteal elastic modulus and followed the same trend of axial > circumferential>radial orientations (Figure 3.4)

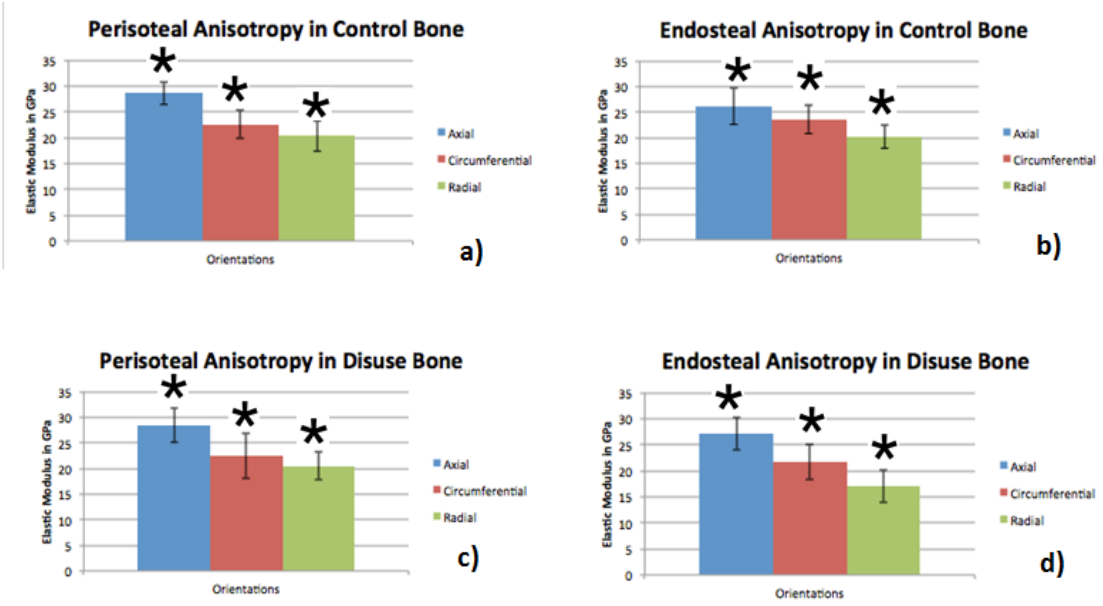

Fig 3.4 (a-b) Graph charts displaying the periosteal and endosteal anisotropy respectively in the control group. (c-d) Graph charts displaying the periosteal and endosteal anisotropy respectively in the disuse group. Statistical analysis performed in ANOVA and significance was set at $\alpha=0.05$.

Variation of Periosteal strength between Control and Experimental groups

On comparing the elastic moduli data at the periosteal region between the control and experimental groups (Figure 3.5), it was observed that there was statistically insignificant difference among the E values for all three orientations i.e. radial ($p>0.05$), circumferential ($p>0.05$) and axial ($p>0.05$).

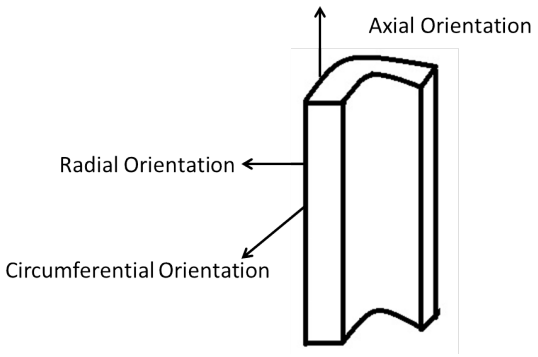

Fig 3.5 Schematic representation of the damage from functional disuse for the periosteal case. The comparison is made between control and experimental groups where a thin arrow represents insignificant damage ($p>0.05$), whereas a thick arrow represents significant damage ($p<0.05$). The image clearly shows insignificant damage in all the three orientations from one month of hind limb suspension.

Variation of Endosteal strength between Control and Experimental groups

On comparing the, the elastic moduli data at the endosteal region between the control and experimental groups (Figure 3.6), statistically significant difference was noted between the E values in radial ($p<0.001$) and circumferential ($p<0.001$) directions. However the difference in the axial direction ($p>0.05$) was statistically insignificant in this respect.

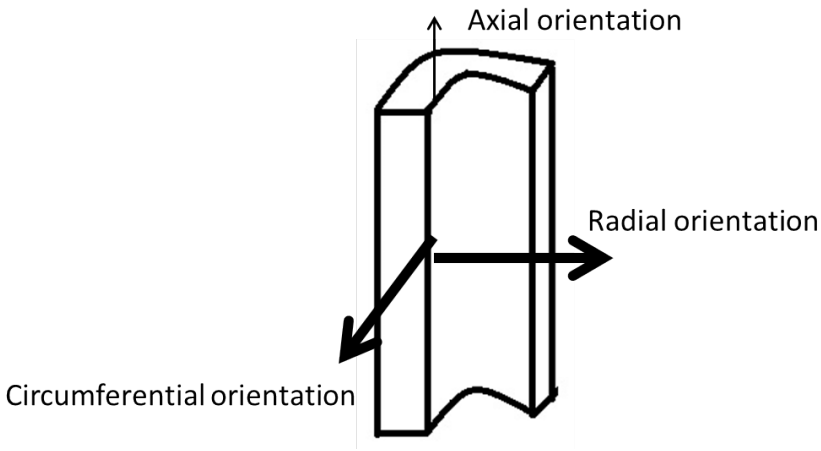

Fig 3.6 Schematic representation of the damage from functional disuse for the endosteal case. The comparison is made between control and experimental groups where a thin arrow represents insignificant damage ($p>0.05$), whereas a thick arrow represents significant damage ($p<0.05$) The image clearly shows significant damage in the circumferential and radial orientations from one month of hind limb suspension.

DISCUSSION

Bone Anisotropy

The elastic modulus values from the control group show that bones had highest strength in the axial direction, which is in agreement with previous research by other groups who used nanoindentation for investigating mechanical strength in the three orthogonal directions (Carnelli et al., 2013; Faingold et al., 2014; Faingold et al., 2012; Franzoso and Zysset, 2009). Inside the bone, the mineral deposition and the collagen content and fiber orientation determine the strength of bone(Knott and Bailey, 1998; Viguet-Carrin et al., 2006a). Previous studies have shown that bone adapts itself to the mechanical loads it faces and changes its properties accordingly (Frost, 1994; Marzban et al., 2012; Meakin et al., 2014; Wolf, 1995). In this study both the periosteum and endosteum regions investigated had a higher axial strength, followed by circumferential and radial orientations. Though bone is formed at the periosteal side and resorbed at the endosteum,

but a similar anisotropy hints out that both sides of the bone experience a highest axial load and a lowest radial oriented load. This strength anisotropy is in agreement with some of the results on the macro scale where a load anisotropy has been shown to be present (Cristofolini et al., 2013; Funk and Crandall, 2006).

The elastic modulus values of the disuse bone clearly highlight the detrimental effects on magnitude of bone strength. But the presence of a similar trend in anisotropy for the functional disuse group as compared to the control shows that though remodeling due to disuse alters the magnitude of bone strength, the orientation of collagen fiber as well as hydroxyapatite mineral crystals might not have changed significantly during the periods of initial damage from osteoporosis. It is previously indicated that osteoporotic conditions lead to poorer collagen fiber organization as well as decreased collagen content in demineralized bones (Silva et al., 2006). The nanoindentation results in this study suggest that osteoporotic conditions might initially lead to reduction in collagen content than an initial poorer collagen fiber organization. Osteoporotic conditions lead to decrease in bone mineral density as well as change in hydroxyapatite mineral dimensions (Faibish et al., 2006). The study suggests that an initial decrease in bone mineral density is more probable than an initial change in dimensions of mineral crystals in the disuse bone. Though a month span is not a very long time period and therefore the results suggest that initial remodeling affects the amount of bone than the structure of bone itself.

Variation of Periosteal strength between Control and Experimental groups

The results of the present study show that between the control and experimental groups, in all the three orientations, there is no statistically significant difference between the micro-mechanical periosteal strength. Previous research on the macro scale shows that damage due to

disuse causes a loss of mechanical strength due to alteration and reduction in mineral deposition, and an alteration in collagen fiber density and strength. In this study, separately investigating the periosteal region shows that its strength in all orientations is unaffected. A plausible explanation can be that remodeling activities from disuse conditions have not affected the periosteal regions in a month. Another pathway for the periosteum to have an unaltered strength is for either the mineralization phase or the collagenous protein phase to compensate for the reduction in the other as the mineral and the protein phase together provide the bone its mechanical competence. Separate studies on deproteinized and demineralized bones need to be conducted which might provide a better insight.

Variation of Endosteal strength between Control and Experimental groups

Damage on the endosteal side, in terms of reduction in micro elastic moduli, hints towards possible resorption of the bone on this side. This is in agreement with much of previous work which shows that damage due to disuse causes endosteal resorption. Our results also signify that there is a specific preferred orientation of damage at the endosteal side. Damage from a micro-mechanical perspective takes place in circumferential and radial or more importantly it does not take place in the axial direction or at least not from one month of functional disuse. Previous studies illustrate that osteocytes, which are the load sensing cells of the bone, sense load also by substrate adhesion (Litzenberger et al., 2010) in addition to the fluid flow mechanism of the interstitial fluid. It might be that osteocytes still experience a substrate adhesion force perpendicular to the cross section. This can be an explanation for remodeling activities not reducing strength across the axial orientation. Another explanation for the orientation specific damage could be the change in endosteal micro-architecture in terms of a change in collagen fiber or mineral crystal organizations and dimensions at the endosteum. The

change in micro-architecture still provides the ability to bear loads in axial orientation but a reduced strength in circumferential and radial load bearing or torsional load bearing ability. The results hint that initial remodeling activity inside the cortical mid-diaphysis has directional properties. The results of this study signify that osteopenia causes bone damage initially on the endosteal region and probably it is the bone resorption pathways and not the bone formation pathways, which are initially affected from bone disuse. This conclusion can be useful for drug designing, as the drugs need to be designed against more for the bone resorption. Initial extra bone formation may not be required.

CONCLUSION

This study suggests that bone has a definite anisotropy in strength in different orientations in the micron scale with the axial or the main load bearing orientation having the maximum strength at both the periosteal and endosteal surfaces. A similar anisotropy in strength is maintained even in one- month old functional disuse bones thus marking anisotropy, as a fundamental property of bone's mechanical behavior. Damage due to disuse begins on the endosteal side of bone. Furthermore the damage begins in the circumferential and radial orientations or the axial orientation is unaffected in the micron scale from a month of functional disuse.

Chapter 4- Work in Progress, Clinical Significances, Limitations of Present Study and Future Directions

Current study showed that material properties inside the cross-section of a bone are correlated to the strain distribution at the same cross section. The cortical mid-diaphysis was investigated in the study. To further confirm the study finite element analysis can be used to

determine the neutral axis for the same cross section. FEA would be a step further in the confirmation of how the strain distribution is varied inside the bone. In this direction bone models were made for the three additional rat tibias, which were used for calculating the strain. The bone models were built in MIMICS by Materialise Inc.

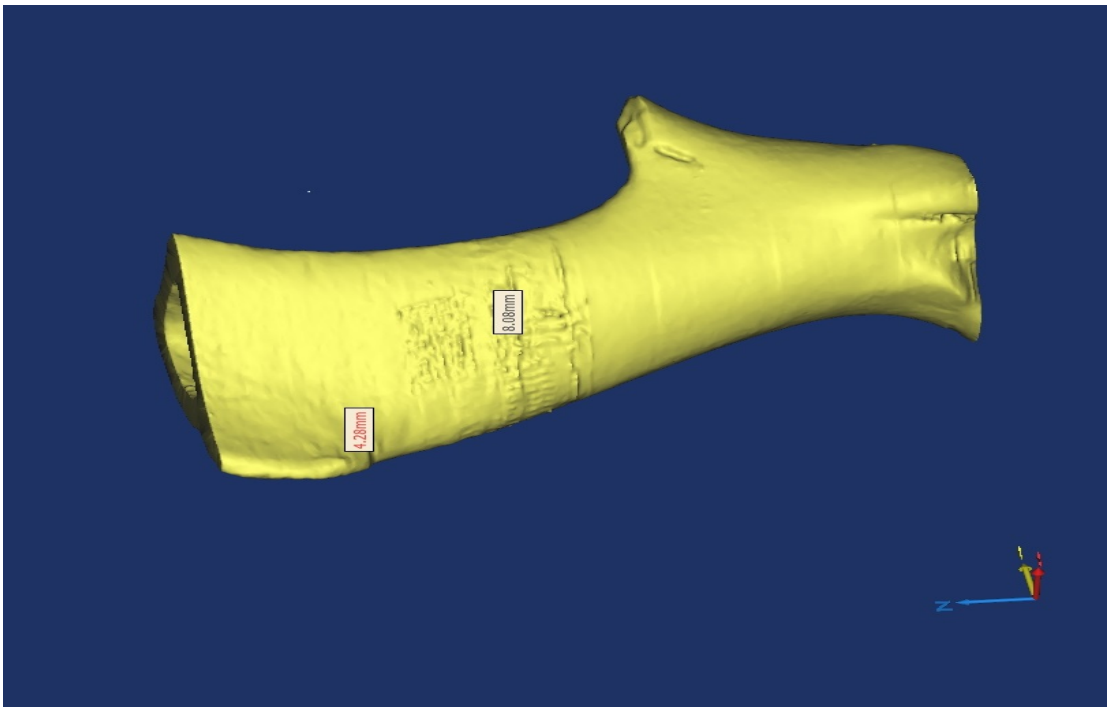

Fig 4.1 Computational rat tibia bone model built in MIMICS

Further meshing of the bone model was done in 3MATIC, which is included in the MIMICS package. The computational bone model was further imported in ABAQUS for FEA.

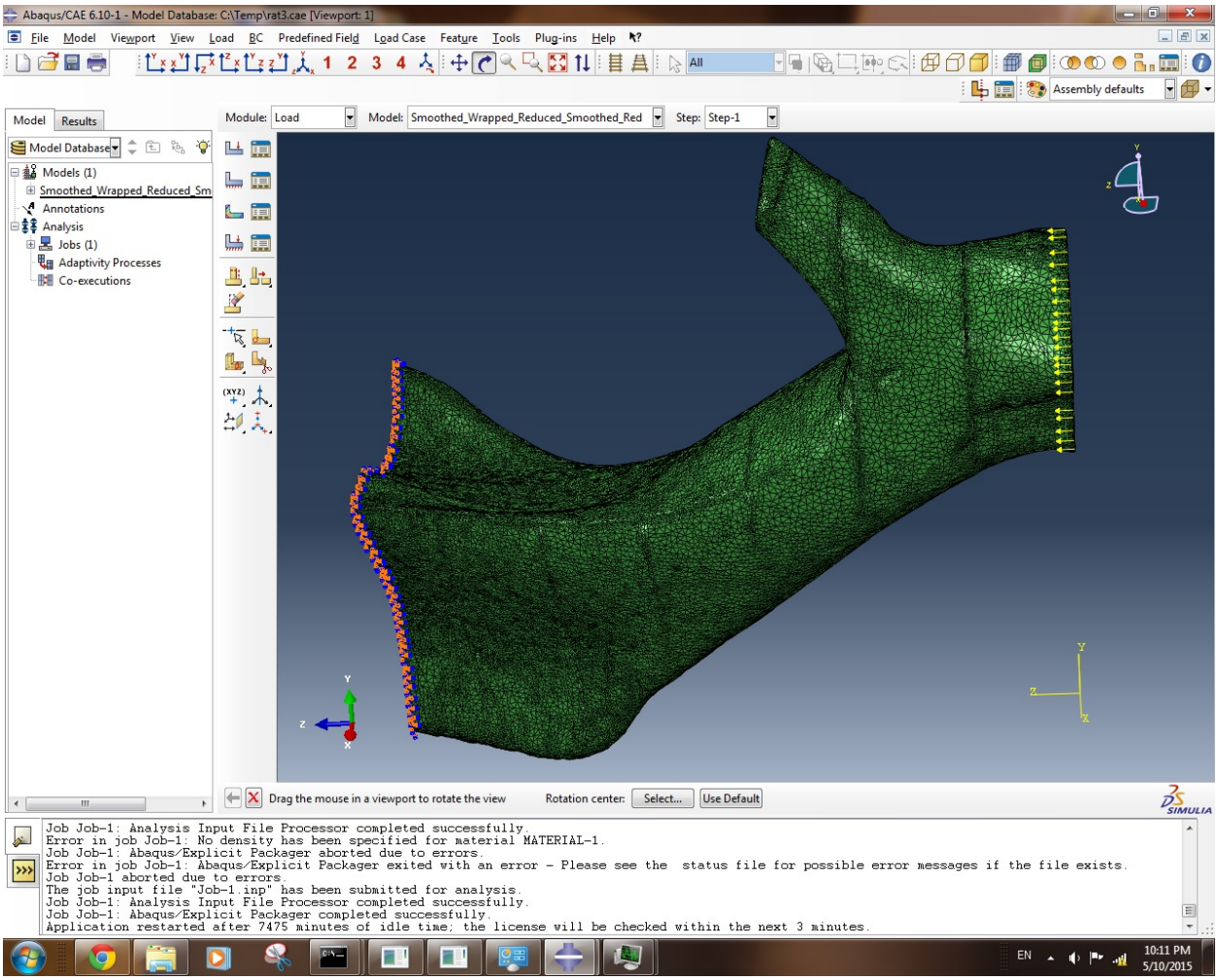

Fig 4.2- Computational rat tibia model loaded in Abaqus for further FEA analysis

The first study could potentially have a high clinical impact. The in vitro and ex vivo studies conducted show that micro mechanical moduli distribution is regionally affected due to functional disuse. Combined with reference point indentation which makes indentation possible without the actual sectioning of bones, a possible clinical diagnostic method can be formulated for osteopenia. The second study presents mechanical data in a micro regime for a possible view on the 3D remodeling activity inside the bone. The mode of mechanical testing is quasi-static nanoindentation at specific sites. Quasi-static nanoindentation gives mechanical parameters of the samples such as elastic modulus and hardness. This is a valid test of elasticity for elastic

materials. However, the main phase inside the bone is the protein phase which is composed of collagen fibers and also responsible for the mechanical properties of bone (Sroga and Vashishth, 2012; Viguet-Carrin et al., 2006b). The collagen fibers are viscoelastic in nature and hence an elastic test such as quasi-static indentation does not provide a complete picture of its mechanical properties (Gautieri et al., 2012). To assess the mechanical properties of bone, which is composed of collagen fibers in various orientations as well as micro- voids, dynamic module indentation is a better option so as to find out both the storage as well as loss modulus to get a complete picture of how does the bone mechanical competence changes spatially (Pathak et al., 2011b).

Next, to further classify anisotropy in different regions and why and how it changes upon bone disuse, one of the possible future directions of work can be to analyze the anisotropy of the respective regions upon demineralizing and deproteinizing the bone. This can give a complete picture about which phase undergoes damage and in which orientation. A step further in this direction can be to assess the collagen fiber orientation at both the periosteum and endosteum sides before and after disuse as collagen fiber orientation has a direct effect on the bone mechanical properties (Bromage et al., 2003). Similarly for investigating bone mineral density distribution, the way can be back scatter electron imaging at the nanoidnetation sites and investigating the distribution of mineral density for the control sample at both periosteum and endosteum (Boskey, 2006). Similar studies can then be conducted for the experimental group.

Some other limitations which are common for both the groups include- 1) The use of a hind limb suspended model for disuse osteopenia. During hind limb suspension the bone, such as the tibia bone in our study, is still susceptible to muscular contraction forces. Hence there is a limitation for it to be considered as a functional disuse model. 2) Embedding the samples in

epoxy requires first the dehydration of the sample. Dehydrating the bones cause an increase in the stiffness of bone(Lewis and Nyman, 2008). Hence this is a limitation for any indentation experiment. An indentation with a fluid cell type indenter can be used to overcome this limitation by indenting hydrated samples not embedded in epoxy resin.

REFERENCES

Angker, L., Swain Mv Fau - Kilpatrick, N., Kilpatrick, N., 2005. Characterising the micro-mechanical behaviour of the carious dentine of primary teeth using nano-indentation. J Biomech 38, 1535-1542.

Bonney, H., Colston Bj Fau - Goodman, A.M., Goodman, A.M., 2011. Regional variation in the mechanical properties of cortical bone from the porcine femur. Med Eng Phys. 33, 513-520.

Boskey, A.L., 2006. Assessment of bone mineral and matrix using backscatter electron imaging and FTIR imaging. Curr Osteoporos Rep 4, 71-75.

Bromage, T.G., Goldman Hm Fau - McFarlin, S.C., McFarlin Sc Fau - Warshaw, J., Warshaw J Fau - Boyde, A., Boyde A Fau - Riggs, C.M., Riggs, C.M., 2003. Circularly polarized light standards for investigations of collagen fiber orientation in bone. Anat Rec B New Anat 274, 157-168.
Burger, E.H., Klein-Nulend, J., 1999. Mechanotransduction in bone--role of the lacuno-canalicular network. FASEB J. 13, 101-112.
Carnelli, D., Vena P Fau - Dao, M., Dao M Fau - Ortiz, C., Ortiz C Fau - Contro, R., Contro, R., 2013. Orientation and size-dependent mechanical modulation within individual secondary osteons in cortical bone tissue. J R Soc Interface 10.
Carter, D.R., 1982. The relationship between in vivo strains and cortical bone remodeling. Crit rev Biomed Eng. 8, 1-28.
Clarke, B., 2008. Normal bone anatomy and physiology. Clin J Am Soc Nephrol 3, 131-139.
Courtland, H.W., Nasser P Fau - Goldstone, A.B., Goldstone Ab Fau - Spevak, L., Spevak L Fau - Boskey, A.L., Boskey Al Fau - Jepsen, K.J., Jepsen, K.J., 2008. Fourier transform infrared imaging microspectroscopy and tissue-level mechanical testing reveal intraspecies variation in mouse bone mineral and matrix composition. Calcif Tissue Int 83, 342-353.
Cristofolini, L., Angeli E Fau - Juszczyk, J.M., Juszczyk Jm Fau - Juszczyk, M.M., Juszczyk, M.M., 2013. Shape and function of the diaphysis of the human tibia. J Biomech 46, 1882-1892.
Currey, J.D., 2003. The many adaptations of bone. J Biomech 36, 1487-1495.
Diez-Perez, A., Guerri R Fau - Nogues, X., Nogues X Fau - Caceres, E., Caceres E Fau - Pena, M.J., Pena Mj Fau - Mellibovsky, L., Mellibovsky L Fau - Randall, C., Randall C Fau - Bridges, D., Bridges D Fau - Weaver, J.C., Weaver Jc Fau - Proctor, A., Proctor A Fau - Brimer, D., Brimer D Fau - Koester, K.J., Koester Kj Fau - Ritchie, R.O., Ritchie Ro Fau - Hansma, P.K., Hansma, P.K., 2010. Microindentation for in vivo measurement of bone tissue mechanical properties in humans. J Bone Miner Res. 25, 1877-1885.
Donaldson Cl Fau - Hulley, S.B., Hulley Sb Fau - Vogel, J.M., Vogel Jm Fau - Hattner, R.S., Hattner Rs Fau - Bayers, J.H., Bayers Jh Fau - McMillan, D.E., McMillan, D.E., 1970. Effect of prolonged bed rest on bone mineral. Metabolism. 19, 1071-1084.
Donnelly, E., Boskey Al Fau - Baker, S.P., Baker Sp Fau - van der Meulen, M.C.H., van der Meulen, M.C., 2010. Effects of tissue age on bone tissue material composition and nanomechanical properties in the rat cortex. J Biomed Mater Res A 92, 1048-1056.
Dwek, J.R., 2010. The periosteum: what is it, where is it, and what mimics it in its absence? Skeletal Radiol 39, 319-323.

Ebenstein, D.M., Pruitt, L.A., 2004. Nanoindentation of soft hydrated materials for application to vascular tissues. J Biomed Mater res A 69, 222-232.
Engelke, K., Libanati C Fau - Fuerst, T., Fuerst T Fau - Zysset, P., Zysset P Fau - Genant, H.K., Genant, H.K., 2013. Advanced CT based in vivo methods for the assessment of bone density, structure, and strength. Curr Osteoporosis Rep 11, 246-255.
Faibish, D., Ott, S.M., Boskey, A.L., 2006. Mineral Changes in Osteoporosis A Review. Clinical orthopaedics and related research 443, 28-38.
Faingold, A., Cohen Sr Fau - Wagner, H.D., Wagner, H.D., 2012. Nanoindentation of osteonal bone lamellae. J Mech Behav Biomed Mater 9, 198-206.
Faingold, A., Cohen, S.R., Shahar, R., Weiner, S., Rapoport, L., Wagner, H.D., 2014. The effect of hydration on mechanical anisotropy, topography and fibril organization of the osteonal lamellae. J Biomech 47, 367-372.
Fan, Z., Swadener Jg Fau - Rho, J.Y., Rho Jy Fau - Roy, M.E., Roy Me Fau - Pharr, G.M., Pharr, G.M., 2002. Anisotropic properties of human tibial cortical bone as measured by nanoindentation. J Orthop Res 20, 806-810.
Franzoso, G., Zysset, P.K., 2009. Elastic anisotropy of human cortical bone secondary osteons measured by nanoindentation. J Biomech Eng 131.
Frost, H.M., 1983. A determinant of bone architecture. The minimum effective strain. Clin Orthop Relat Res., 286-292.
Frost, H.M., 1994. Wolff's Law and bone's structural adaptations to mechanical usage: an overview for clinicians. Angle Orthod 64, 175-188.
Funk, J.R., Crandall, J.R., 2006. Calculation of tibial loading using strain gauges. Biomed Sci Instrum 42, 160-165.
Gallant, M.A., Brown Dm Fau - Organ, J.M., Organ Jm Fau - Allen, M.R., Allen Mr Fau - Burr, D.B., Burr, D.B., 2013. Reference-point indentation correlates with bone toughness assessed using whole-bone traditional mechanical testing. Bone 53, 301-305.
Gautieri, A., Vesentini S Fau - Redaelli, A., Redaelli A Fau - Buehler, M.J., Buehler, M.J., 2012. Viscoelastic properties of model segments of collagen molecules. Matrix Biol 31, 141-149.
Gilsanz, V., 1998. Bone density in children: a review of the available techniques and indications. Eur J Radiol 26, 177-182.
Goldman, H.M., Thomas Cd Fau - Clement, J.G., Clement Jg Fau - Bromage, T.G., Bromage, T.G., 2005. Relationships among microstructural properties of bone at the human midshaft femur. J Anat. 206, 127-139.

Granke, M., Coulmier, A., Uppuganti, S., Gaddy, J.A., Does, M.D., Nyman, J.S., 2014. Insights into reference point indentation involving human cortical bone: sensitivity to tissue anisotropy and mechanical behavior. J Mech Behav Biomed Mater. 37, 174-185.
Gross D Fau - Williams, W.S., Williams, W.S., 1982. Streaming potential and the electromechanical response of physiologically-moist bone. J Biomech 15, 277-295.
Gross, T.S., Rubin, C.T., 1995. Uniformity of resorptive bone loss induced by disuse. J Orthop Res 13, 708-714.
Hakulinen, M.A., Toyras J Fau - Saarakkala, S., Saarakkala S Fau - Hirvonen, J., Hirvonen J Fau - Kroger, H., Kroger H Fau - Jurvelin, J.S., Jurvelin, J.S., 2004. Ability of ultrasound backscattering to predict mechanical properties of bovine trabecular bone. Ultrasound Med Biol 30, 919-927.
Hammond, M.A., Gallant, M.A., Burr, D.B., Wallace, J.M., 2014. Nanoscale changes in collagen are reflected in physical and mechanical properties of bone at the microscale in diabetic rats. Bone 60, 26-32.
Hengsberger, S., Kulik, A., Zysset, P., 2002. Nanoindentation discriminates the elastic properties of individual human bone lamellae under dry and physiological conditions. Bone 30, 178-184.
Hoc, T., Henry L Fau - Verdier, M., Verdier M Fau - Aubry, D., Aubry D Fau - Sedel, L., Sedel L Fau - Meunier, A., Meunier, A., 2006. Effect of microstructure on the mechanical properties of Haversian cortical bone. Bone 36, 466-474.
Hoffler, C.E., Guo Xe Fau - Zysset, P.K., Zysset Pk Fau - Goldstein, S.A., Goldstein, S.A., 2005. An application of nanoindentation technique to measure bone tissue Lamellae properties. J Biomech Eng 127, 1046-1053.
Hoffmeister, B.K., Smith Sr Fau - Handley, S.M., Handley Sm Fau - Rho, J.Y., Rho, J.Y., 2000. Anisotropy of Young's modulus of human tibial cortical bone. Med Biol Eng Comput 38, 333-338.
Hsieh, Y.F., Wang T Fau - Turner, C.H., Turner, C.H., 1999. Viscoelastic response of the rat loading model: implications for studies of strain-adaptive bone formation. Bone 25, 379-382.
Hu, M., Cheng J Fau - Qin, Y.-X., Qin, Y.X., 2012. Dynamic hydraulic flow stimulation on mitigation of trabecular bone loss in a rat functional disuse model. Bone 51.
Hu M, Q.Y., 2014. Dynamic fluid flow stimulation on cortical bone and alterations of the gene expressions of osteogenic growth factors and transcription factors in a rat functional disuse model. Arch Biochem Biophys, 154-161.
Huang, C., Ogawa, R., 2010. Mechanotransduction in bone repair and regeneration. FASEB J 24, 3625-3632.

Huang, C., Ogawa, R., 2013. Mechanotransduction in bone repair and regeneration. Trends Mol Med. 19, 555-564.
Imbert, L., Auregan, J.C., Pernelle, K., Hoc, T., 2011. Mechanical and mineral properties of osteogenesis imperfecta human bones at the tissue level. Med Eng Phys 33, 513-520.
Kaneps, A.J., Stover Sm Fau - Lane, N.E., Lane, N.E., 1997. Changes in canine cortical and cancellous bone mechanical properties following immobilization and remobilization with exercise. Bone 21, 419-423.
Kelly, P.J., Bronk, J.T., 1990. Venous pressure and bone formation. Microvasc Res. 39, 364-375.
Khandaker, M., Ekwaro-Osire, S., 2013. Weibull analysis of fracture test data on bovine cortical bone: influence of orientation. Int J Biomater.
Knothe Tate, M.L., Niederer P Fau - Knothe, U., Knothe, U., 1998. In vivo tracer transport through the lacunocanalicular system of rat bone in an environment devoid of mechanical loading. Bone 22, 107-117.
Knott, L., Bailey, A.J., 1998. Collagen cross-links in mineralizing tissues: a review of their chemistry, function, and clinical relevance. Bone 22, 181-187.
Kodama, Y., Umemura Y Fau - Nagasawa, S., Nagasawa S Fau - Beamer, W.G., Beamer Wg Fau - Donahue, L.R., Donahue Lr Fau - Rosen, C.R., Rosen Cr Fau - Baylink, D.J., Baylink Dj Fau - Farley, J.R., Farley, J.R., 2000. Exercise and mechanical loading increase periosteal bone formation and whole bone strength in C57BL/6J mice but not in C3H/Hej mice. Calcif Tissue Int 66, 298-306.
Kotha, S.P., DePaula Ca Fau - Mann, A.B., Mann Ab Fau - Guzelsu, N., Guzelsu, N., 2008. High frequency ultrasound prediction of mechanical properties of cortical bone with varying amount of mineral content. Ultrasound Med Biol 34, 630-637.
LaMothe, J.M., Hamilton Nh Fau - Zernicke, R.F., Zernicke, R.F., 2005. Strain rate influences periosteal adaptation in mature bone. Med Eng Phys 27, 277-284.
Lanyon, L.E., 1987. Functional strain in bone tissue as an objective, and controlling stimulus for adaptive bone remodelling. J Biomech. 20, 1083-1093.
Lata, P.F., Elliott, M.E., 2007. Patient assessment in the diagnosis, prevention, and treatment of osteoporosis. Nutr Clin Pract 22, 261-275.
Lau, R.Y., Guo, X., 2011. A review on current osteoporosis research: with special focus on disuse bone loss. J Osteoporosis.
Legros, R., Balmain N Fau - Bonel, G., Bonel, G., 1987. Age-related changes in mineral of rat and bovine cortical bone. Calcif Tissue Int. 41, 137-144.

Lewis, G., Nyman, J.S., 2008. The use of nanoindentation for characterizing the properties of mineralized hard tissues: state-of-the art review. J Biomed Mater Res B Appl Biomater 87, 286-301.
Lin, L., Oon Hy Fau - Lin, W., Lin W Fau - Qin, Y.-X., Qin, Y.X., 2014. Principal trabecular structural orientation predicted by quantitative ultrasound is strongly correlated with muFEA determined anisotropic apparent stiffness. Biomech Model Mechanobiol 13, 961-971.
Litzenberger, J.B., Kim Jb Fau - Tummala, P., Tummala P Fau - Jacobs, C.R., Jacobs, C.R., 2010. Beta1 integrins mediate mechanosensitive signaling pathways in osteocytes. Calcif Tissue Int 86, 325-332.
Main, R.P., Lynch Me Fau - van der Meulen, M.C.H., van der Meulen, M.C., 2010. In vivo tibial stiffness is maintained by whole bone morphology and cross-sectional geometry in growing female mice. J Biomech. 43, 2689-2694.
Manske, S.L., Lorincz Cr Fau - Zernicke, R.F., Zernicke, R.F., 2009. Bone health: part 2, physical activity. Sports Health 1, 341-346.
Marzban, A., Canavan P Fau - Warner, G., Warner G Fau - Vaziri, A., Vaziri A Fau - Nayeb-Hashemi, H., Nayeb-Hashemi, H., 2012. Parametric investigation of load-induced structure remodeling in the proximal femur. Proc Inst Mech Eng H 226, 450-460.
McLeod, K.J., Rubin Ct Fau - Otter, M.W., Otter Mw Fau - Qin, Y.X., Qin, Y.X., 1998. Skeletal cell stresses and bone adaptation. Am J Med Sci. 316, 176-183.
McPherson, J.G., Edwards, W.B., Prasad, A., Troy, K.L., Griffith, J.W., Schnitzer, T.J., 2014. Dual energy X-ray absorptiometry of the knee in spinal cord injury: methodology and correlation with quantitative computed tomography. LID - 10.1038/sc.2014.122 [doi]. Spinal Cord.
Meakin, L.B., Price, J.S., Lanyon, L.E., 2014. The Contribution of Experimental in vivo Models to Understanding the Mechanisms of Adaptation to Mechanical Loading in Bone. Front Endocrinol 5.
Patel, T.K., Brodt, M.D., Silva, M.J., 2014. Experimental and finite element analysis of strains induced by axial tibial compression in young-adult and old female C57Bl/6 mice. J Biomech 47, 451-457.
Pathak, S., Swadener Jg Fau - Kalidindi, S.R., Kalidindi Sr Fau - Courtland, H.-W., Courtland Hw Fau - Jepsen, K.J., Jepsen Kj Fau - Goldman, H.M., Goldman, H.M., 2011a. Measuring the dynamic mechanical response of hydrated mouse bone by nanoindentation. J Mech Behav Biomed Mater. 4, 34-43.
Pathak, S., Swadener Jg Fau - Kalidindi, S.R., Kalidindi Sr Fau - Courtland, H.-W., Courtland Hw Fau - Jepsen, K.J., Jepsen Kj Fau - Goldman, H.M., Goldman, H.M., 2011b. Measuring the dynamic mechanical response of hydrated mouse bone by nanoindentation. J Mech Behav Biomed Mater 4, 34-43.

Pathak, S., Vachhani Sj Fau - Jepsen, K.J., Jepsen Kj Fau - Goldman, H.M., Goldman Hm Fau - Kalidindi, S.R., Kalidindi, S.R., 2012a. Assessment of lamellar level properties in mouse bone utilizing a novel spherical nanoindentation data analysis method. J Mech Behav Biomed Mater 13, 102-117.
Pathak, S., Vachhani Sj Fau - Jepsen, K.J., Jepsen Kj Fau - Goldman, H.M., Goldman Hm Fau - Kalidindi, S.R., Kalidindi, S.R., 2012b. Assessment of lamellar level properties in mouse bone utilizing a novel spherical nanoindentation data analysis method. J Mech Behav Biomed Mater. 13, 102-117.
Pekka, M., 2007. Muscles. Merck Manual.
Qin, Y.X., Kaplan T Fau - Saldanha, A., Saldanha A Fau - Rubin, C., Rubin, C., 2003. Fluid pressure gradients, arising from oscillations in intramedullary pressure, is correlated with the formation of bone and inhibition of intracortical porosity. J Biomech. 36, 1427-1437.
Qin, Y.X., Lam H Fau - Ferreri, S., Ferreri S Fau - Rubin, C., Rubin, C., 2010. Dynamic skeletal muscle stimulation and its potential in bone adaptation. J Musculoskeletal Neuronal Interact. 10, 12-24.
Qin, Y.X., Lin W Fau - Mittra, E., Mittra E Fau - Xia, Y., Xia Y Fau - Cheng, J., Cheng J Fau - Judex, S., Judex S Fau - Rubin, C., Rubin C Fau - Muller, R., Muller, R., 2013. Prediction of trabecular bone qualitative properties using scanning quantitative ultrasound. Acta Astronaut. 92, 79-88.
Qin, Y.X., Rubin Ct Fau - McLeod, K.J., McLeod, K.J., 1998. Nonlinear dependence of loading intensity and cycle number in the maintenance of bone mass and morphology. J Orthop Res. 16, 482-489.
Ramasamy, J.G., Akkus, O., 2007. Local variations in the micromechanical properties of mouse femur: the involvement of collagen fiber orientation and mineralization. J Biomech. 40, 910-918.
Reich, K.M., Gay Cv Fau - Frangos, J.A., Frangos, J.A., 1990. Fluid shear stress as a mediator of osteoblast cyclic adenosine monophosphate production. J Cell Physiol. 143, 100-104.
Reisinger, A.G., Pahr Dh Fau - Zysset, P.K., Zysset, P.K., 2011. Principal stiffness orientation and degree of anisotropy of human osteons based on nanoindentation in three distinct planes. J Mech Behav Biomed Mater 4, 2113-2127.
Rho, J.Y., Kuhn-Spearing L Fau - Zioupos, P., Zioupos, P., 1998. Mechanical properties and the hierarchical structure of bone. Med Eng Phys 20, 92-102.
Rubin Ct Fau - Lanyon, L.E., Lanyon, L.E., 1987. Kappa Delta Award paper. Osteoregulatory nature of mechanical stimuli: function as a determinant for adaptive remodeling in bone. J Orthop Res. 5, 300-310.
Rubin, J., Biskobing D Fau - Fan, X., Fan X Fau - Rubin, C., Rubin C Fau - McLeod, K., McLeod K Fau - Taylor, W.R., Taylor, W.R., 1997. Pressure regulates osteoclast formation and MCSF expression in marrow culture. J Cell Physiol. 170, 81-87.

Ryan, C.S., Petkov Vi Fau - Adler, R.A., Adler, R.A., 2011. Osteoporosis in men: the value of laboratory testing. Osteoporosis Int 22, 1845-1853.
Seeman, E., 2003. Reduced bone formation and increased bone resorption: rational targets for the treatment of osteoporosis. Osteoporos Int 14.
Serra-Hsu, F., Cheng J Fau - Lynch, T., Lynch T Fau - Qin, Y.-X., Qin, Y.X., 2011. Evaluation of a pulsed phase-locked loop system for noninvasive tracking of bone deformation under loading with finite element and strain analysis. Physiol Meas. 32, 1301-1313.
Silva, M.J., Brodt Md Fau - Fan, Z., Fan Z Fau - Rho, J.-Y., Rho, J.Y., 2004. Nanoindentation and whole-bone bending estimates of material properties in bones from the senescence accelerated mouse SAMP6. J Biomech. 37, 1639-1646.
Silva, M.J., Brodt Md Fau - Wopenka, B., Wopenka B Fau - Thomopoulos, S., Thomopoulos S Fau - Williams, D., Williams D Fau - Wassen, M.H.M., Wassen Mh Fau - Ko, M., Ko M Fau - Kusano, N., Kusano N Fau - Bank, R.A., Bank, R.A., 2006. Decreased collagen organization and content are associated with reduced strength of demineralized and intact bone in the SAMP6 mouse. J Bone Miner Res. 21, 78-88.
Skedros, J.G., Hunt, K.J., 2004. Does the degree of laminarity correlate with site-specific differences in collagen fibre orientation in primary bone? An evaluation in the turkey ulna diaphysis. J Anat. 205, 121-134.
Skedros, J.G., Hunt Kj Fau - Bloebaum, R.D., Bloebaum, R.D., 2004. Relationships of loading history and structural and material characteristics of bone: development of the mule deer calcaneus. J Morphol. 259, 281-307.
Sroga, G.E., Vashishth, D., 2012. Effects of bone matrix proteins on fracture and fragility in osteoporosis. Curr Osteoporos Rep 10, 141-150.
Szulc, P., Seeman E Fau - Duboeuf, F., Duboeuf F Fau - Sornay-Rendu, E., Sornay-Rendu E Fau - Delmas, P.D., Delmas, P.D., 2006. Bone fragility: failure of periosteal apposition to compensate for increased endocortical resorption in postmenopausal women. J Bone Miner Res 21, 1856-1863.
Torcasio, A., Zhang X Fau - Duyck, J., Duyck J Fau - van Lenthe, G.H., van Lenthe, G.H., 2012. 3D characterization of bone strains in the rat tibia loading model. Biomech Model Mechanobiol 11, 403-410.
Turner, C.H., Forwood Mr Fau - Otter, M.W., Otter, M.W., 1994. Mechanotransduction in bone: do bone cells act as sensors of fluid flow? FASEB J 8, 875-878.

van der Meulen, M.C., Morgan Tg Fau - Yang, X., Yang X Fau - Baldini, T.H., Baldini Th Fau - Myers, E.R., Myers Er Fau - Wright, T.M., Wright Tm Fau - Bostrom, M.P.G., Bostrom, M.P., 2006. Cancellous bone adaptation to in vivo loading in a rabbit model. Bone 38, 871-877.
Ved, N., Haller, J.O., 2002. Periosteal reaction with normal-appearing underlying bone: a child abuse mimicker. Emerg Radiol. 9, 278-282.
Viguet-Carrin, S., Garnero P Fau - Delmas, P.D., Delmas, P.D., 2006a. The role of collagen in bone strength. Osteoporosis Int 17, 319-336.
Viguet-Carrin, S., Garnero P Fau - Delmas, P.D., Delmas, P.D., 2006b. The role of collagen in bone strength. Osteoporos Int 17, 319-336.
Wallace, J.M., Ron Ms Fau - Kohn, D.H., Kohn, D.H., 2009. Short-term exercise in mice increases tibial post-yield mechanical properties while two weeks of latency following exercise increases tissue-level strength. Calcif Tissue Int 84, 297-304.
Weinbaum, S., Cowin Sc Fau - Zeng, Y., Zeng, Y., 1994. A model for the excitation of osteocytes by mechanical loading-induced bone fluid shear stresses. J Biomech. 27, 339-360.
Weiner, S., Traub W Fau - Wagner, H.D., Wagner, H.D., 1999. Lamellar bone: structure-function relations. J Struct Biol 30, 241-255.
Weryha, G., Leclere J Fau - Regent, D., Regent, D., 1991. [Bone densitometry: technical principles and practical value]. Ann Endocrinol 52, 298-304.
Wolf, J.H., 1995. [Julis Wolff and his "law of bone remodeling"]. Orthopade. 24, 378-386.
Xing, X.P., Xia Wb Fau - Meng, X.-w., Meng Xw Fau - Zhou, X.-y., Zhou Xy Fau - Hu, Y.-y., Hu Yy Fau - Liu, H.-c., Liu, H.C., 2003. [Evaluation of bone architecture and biomechanic properties by peripheral quantitative computed tomography in rats]. Zhonghua Yi Xue Za Zhi 83, 791-795.
Zeng, Y., Cowin Sc Fau - Weinbaum, S., Weinbaum, S., 1994. A fiber matrix model for fluid flow and streaming potentials in the canaliculi of an osteon. Ann Biomed Eng. 22, 280-292.

References of Figures-

Fig 1.1

https://www.tumblr.com/search/compact%20bone

Fig 1.2

http://bm3.unl.edu/hysitron-nanoindenter